# THE GEOPHYSICAL CRUST-TO-MANTLE TRANSITION FROM RECEIVER FUNCTION ANALYSIS: A CASE STUDY ON THE APPALACHIAN FRONT IN QUEBEC, CANADA

By

BENJAMIN DUNHAM

A thesis submitted to the

Graduate School-New Brunswick

Rutgers, The State University of New Jersey

For the degree of

Master of Science

Graduate Program in Geological Sciences

Written under the direction of

Dr. Vadim Levin

And approved by

_____

_____

_____

New Brunswick, New Jersey

January, 2017

ABSTRACT OF THE THESIS

The Geophysical Crust-to-Mantle Transition from Receiver Function Analysis: A case Study on the Appalachian Front in Quebec, Canada

by BENJAMIN DUNHAM

Thesis Director:

Vadim Levin

Receiver function analysis is useful for studying relative variations of seismic discontinuities at the lithospheric scale. This study uses receiver functions computed from a densely spaced 2D grid of six receivers that collected passive seismic data over a decade in the lower St. Lawrence River, Quebec, Canada. The lower crustal structure and lithospheric mantle are not well constrained in this study area, which is centered on the tectonic boundary between the Grenville and Appalachian provinces. Thus, the goals of this study are: 1) to establish the consistency and resolution limits of receiver functions from a large data set and dense permanent array of receivers; and 2) to use this grid to identify the geophysical Moho and describe the lithospheric mantle-to-crust transition across the Appalachian front (AF), the western boundary of Appalachian deformation.

The relative seismic velocity changes under the AF resolved by Receiver Function Analysis provide evidence of local variability in the Moho's depth and sharpness. Frequency-based analysis of the receiver functions in the northwest region of the study area produces variable Moho depth estimates from 50 to 35 km, and exhibits a gradational transition from the crust to the mantle. In the southeast region, the Moho has more consistent depth and is sharper. The likely cause of this variability is either deep-

reaching shear zones that offset the Moho, or a high-velocity layer in the lower crust that is only apparent in areas where it produces significant impedance contrasts between layers.

ACKNOWLEDGEMENTS

Completion of this thesis research would not have been possible without the constant support and supervision of my thesis advisor, Vadim Levin. I cannot possibly express my full gratitude for his professional and personal support.

I also need to thank my parents, Robin and Dave Dunham, as well as my siblings Dave, Annie and Nicholas for always being available when I needed them. The faculty and staff of the Earth and Planetary Sciences Department provided me with the support, foundation and education that influenced me as person and scientist. I extend my deepest gratitude to the graduate students (both past and present) that have helped me through the duration of my time as graduate student. Thanks to Catherine Beck, Selene Esmeray Senlet, Jesse Thornburg, Chris Vidito, Margot Ferenz and Cesar Sequeira for shaping my undergraduate education as teaching assistants. Thank you to the graduate students I have had the opportunity to grow with, Lindsey Lugrin, Xiaoren Chen, Natalie Stier, Max Needle, Ryan Hupfer, Rachel Filo, Gabe Gallegos, Chris Johnson and Jake Setera, Ayda Razi, Masha Makarova.

I would also like to thank Adrian Howansky, Sean Kinney, and Bill Reilly for their friendship and support.

Finally thank you to the students and student researchers who provided input and feedback on my thesis research, Cesar Sequeira, Andrea Servali and Michael Klaser, as well as the developers of the open source software necessary for processing the data for this research, GMT, SAC and the TauP Toolkit.

Table of Contents


| | Page |
|---|---|
| Title Page | i |
| Abstract | ii |
| Acknowledgements | iv |
| Table of Contents | v |
| List of Illustrations | viii |
| 1. Introduction | 1 |
| 1.1. Goal | 1 |
| 1.2. Study Region and Targets | 2 |
| 1.3. Geologic History and Geophysical Properties | 2 |
| 1.3.1. Grenville | 3 |
| 1.3.2. Iapetan Rift | 4 |
| 1.3.3. Appalachians | 5 |
| 1.4. Summary | 5 |
| 2. Data Description | 6 |
| 3. Methods | 7 |
| 3.1. Receiver Function Applications | 7 |
| 3.2. Basic Earthquake Physics | 8 |
| 3.3. Receiver Function Theory | 9 |
| 3.4. Study Area Description | 10 |
| 3.5. Receiver Function Modeling | 11 |
| 4. Results | 15 |

4.1. Site A11 16

4.1.1. Epicentral Receiver Function, Baz 300°-350° 16

4.2. Site A16 17

4.2.1. Epicentral Receiver Function, Baz 300°-350° 18

4.2.2 Epicentral Receiver Function, Baz 15°-75° 18

4.2.3. Epicentral Receiver Function, Baz 164°-195° 19

4.3. Site A21 20

4.3.1 Epicentral Receiver Function, Baz 300°-350° 20

4.3.2. Epicentral Receiver Function, Baz 170°-200° 21

4.4. Site A54 22

4.4.1 Epicentral Receiver Function, Baz 300°-350° 22

4.4.2. Epicentral Receiver Function, Baz 30°-50° 23

4.4.3. Epicentral Receiver Function, Baz 180°-190° 23

4.5. Site A61 24

4.5.1 Epicentral Receiver Function, Baz 310°-340° 24

4.5.2. Epicentral Receiver Function, Baz 20°-80° 25

4.5.3. Epicentral Receiver Function, Baz 170°-190° 26

4.6. Site A64 26

4.6.1. Epicentral Receiver Function, Baz 300°-350° 27

4.6.2. Epicentral Receiver Function, Baz 10°-65° 27

4.6.3. Epicentral Receiver Function, Baz 170°-190° 28

4.7. Results Summary 28

5. Discussion 30

5.1. Previous Studies 30

5.2. Moho Relief 32

5.3. Thin Layer 33

5.4. Complex Crust-to-Mantle Transition Zone 35

6. Conclusions 35

7. Bibliography 38

List of Illustrations

1. Regional and Local Map of the Study Area 41

2. Four Phase Tectonic History of the St. Lawrence River 42

3. Map of Sources Used to compute RFs at Site A11 43

4. Map of Sources Used to compute RFs at Site A16 44

5. Map of Sources Used to compute RFs at Site A21 45

6. Map of Sources Used to compute RFs at Site A54 46

7. Map of Sources Used to compute RFs at Site A61 47

8. Map of Sources Used to compute RFs at Site A64 48

9. Schematic Diagram of Receiver Function Geometry and Seismograms 49

10. Ray path geometry of modeled P-waves 50

11. Crustal Velocity Vs. Depth Graph 51

12. Velocity Vs. Depth Graph of the Modeled ak-135 Whole-Earth Velocity Model 52

13. Map of Receiver Ps Conversion Locations at the Base of the Crust 53

14. Time to Depth Conversion Procedure 54

15. Map of Receivers and Time Delays From RF interpretations 55

16. Back-Azimuth Receiver Function Gathers at Site A11 56

17. Interpreted Epicentral Receiver Functions at Site A11 Filtered Below 1 Hz 57

18. Interpreted Epicentral Receiver Functions at Site A11 Filtered Below 2 Hz 58

19. Back-Azimuth Receiver Function Gathers at Site A16 59

20. Interpreted Epicentral Receiver Functions at Site A16 Filtered Below 1 Hz 60

21. Interpreted Epicentral Receiver Functions at Site A16 Filtered Below 2 Hz 61

22. Back-Azimuth Receiver Function Gathers at Site A21 62

23. Interpreted Epicentral Receiver Functions at Site A21 Filtered Below 1 Hz 63

24. Interpreted Epicentral Receiver Functions at Site A21 Filtered Below 2 Hz 64

25. Back-Azimuth Receiver Function Gathers at Site A54 65

26. Interpreted Epicentral Receiver Functions at Site A54 Filtered Below 1 Hz 66

27. Interpreted Epicentral Receiver Functions at Site A54 Filtered Below 2 Hz 67

28. Back-Azimuth Receiver Function Gathers at Site A61 68

29. Interpreted Epicentral Receiver Functions at Site A61 Filtered Below 1 Hz 69

30. Interpreted Epicentral Receiver Functions at Site A61 Filtered Below 2 Hz 70

31. Back-Azimuth Receiver Function Gathers at Site A64 71

32. Interpreted Epicentral Receiver Functions at Site A64 Filtered Below 1 Hz 72

33. Interpreted Epicentral Receiver Functions at Site A64 Filtered Below 2 Hz 73

34. Depth Estimate Map of Single Pulses and Late Arrival of Double Pulses 74

35. Depth Estimate Map of Single Pulses and Early Arrival of Double Pulses 75

36. Cross Sections Across and Along the Appalachian Front 76

# 1. Introduction

## 1.1. Goal

The continental Mohorovicic discontinuity (Moho) is a globally recognizable geophysical feature that exhibits a rapid change in seismic wave velocity across it. It marks the transition from the lower velocity and density, silica-rich crustal material above to higher velocity and density, ultramafic mantle material below (e.g., Cook et al., 2010). The depth and sharpness of the Moho can vary greatly. Globally, the depth of the continental Moho may vary from 30 to 80 km below the Earth's surface (e.g., Cook et al., 2010; Eaton, 2006).

The Appalachian and Grenville provinces (Fig. 1) are stable crustal regions, geologically inactive for the last ~200 Ma. These two provinces meet at the Appalachian Front (AF) where Appalachian deformation ends and Grenville aged deformation begins. Previous geophysical studies on the crust-to- mantle transition below the Appalachian and Grenville terranes and across the AF have produced variable depth estimates that are generally unexpected in regions with old and stable continental crust. The Moho is more obvious to the west under the Grenville terrane than in the AF. Studies that have focused on the Moho structure under the northern Appalachians have proposed shallowing of the Moho to the east (e.g. Li et al., 2002).

Difficulties observing the Moho and its properties in this region are likely related to the complex geological history of the St. Lawrence region. Crustal thickening during the Grenville orogeny (1100 Ma, Hynes & Rivers, 2010), crustal thinning related to the Iapetan rifting event (~617-550 Ma, Whitmeyer & Karlstrom 2007, Higgins & Van

Breeman, 1998, Kumarapeli 1993), and Appalachian-related subduction and arc magmatism (Fig. 2) have all altered the structure of the Moho here.

### 1.2. Study Region and Targets

Receiver functions (RFs) are a powerful geophysical tool for investigating seismic discontinuities, specifically the Mohorovicic discontinuity (Moho) in this study. The reliability of results from individual receivers depends on the amount of data stacked to produce a receiver function. The six receivers used in this study are closely spaced (~20 km apart) and positioned on opposing banks of the lower St. Lawrence River (Fig. 1). Each receiver has collected data for over a decade. The geometry of this receiver grid and the size of this data set provide a unique opportunity to test the ability of receiver functions computed at different locations with varied orientations to consistently and reliably resolve the Moho over a scale of tens of kilometers. This study aims to constrain the depth and sharpness of the Moho under the geologically complex St. Lawrence River, both across and along the AF.

### 1.3. Geologic History/Geophysical Properties

This region's geologic history involves three different tectonic regimes since the late Proterozoic (Fig. 2). First, crustal shortening occurred as a result of the Grenville orogeny's continent-continent collision from 1,100 to 950 Ma (Hynes and Rivers, 2010), followed by extension related to continental rifting between 617 and 550 Ma

(Kuramapeli, 1993; Higgins & Van Breeman, 1998; Hodych & Cox, 2007); finally, between 485 and 350 Ma, the region's crust underwent shortening again by multiple Appalachian orogenic events (Prave et al., 2000; Whitehead et al., 1996). If and to what extent each deformational event may have influenced the Moho structure at the time of their occurrence is difficult to constrain. At present only the effect of their collective deformation is observable. The Appalachian and Grenville terranes are juxtaposed across the Appalachian Front, located within the St. Lawrence River (Figs. 1 & 2).

### 1.3.1 Grenville

The eastern extent of the Grenville Province's surficial expression is coincident with the western bank of the St. Lawrence River (Fig. 1). The continental collision that formed the Grenville orogen was a part of the construction of Rodinia, the Proterozoic super-continent (Whitmeyer & Karlstrom, 2007) (Fig. 2a). The Himalayas are the only modern example of continent-continent collisions. Crustal thickness of Himalayas is 80 km in some places (e.g. Razi et al., 2014). The Grenville Province has undergone erosion over last 1,100 Ma leaving metamorphic mid to lower crustal rocks exposed due to removal of the overlying crustal material and isostatic uplift. The Moho depth under the Grenville province, estimated in previous refraction, reflection and teleseismic receiver function studies, is between 34 and 54 km (Cook et al., 2010; Eaton et al., 2006; Thomson et al., 2015). Exposures of medium to high grade metamorphic rocks indicate that the crust has thinned significantly since Grevillian deformation.

### 1.3.2 Iapetan Rift

The St. Lawrence River and Logan's line mark the AF, boundary between Proterozoic Grenville and Paleozoic Appalachian deformation (Alkok, 1945). This region became the central axis of the Iapetan rifting following the formation of Rodinia (Whitemeyer & Karlstrom 2007, Higgins & Van Breeman, 1998, Kumarapeli 1993). Petrologic evidence from dated dikes, lava flows and layered mafic intrusions suggest Iapetan rifting and eventual drift was triggered by mantle-plume magmatism (Kuramapeli, 1993; Higgins & Van Breeman, 1998; Hodych & Cox, 2007). Either a single long-lived mantle plume (Hodych & Cox, 2007) or possibly two in quick succession (Higgins & Van Breeman, 1998) created a rift-rift-rift triple-junction, that transitioned from rifting to drifting sometime between 617 and 550 Ma (Kuramapeli, 1993; Higgins & Van Breeman, 1998; Hodych & Cox, 2007). This event would likely have thinned the continental crust above it, eventually transitioning from continental to oceanic crust compositions during seafloor spreading at the onset of continental drift. The marine sedimentary sequences thrust on top of the Grenville basement during the Appalachian Taconic deformation (485-440 Ma, Prave et al., 2000) indicate the region became a stable oceanic shelf between the emplacement of Grenville and Appalachian terranes (Whitehead et al., 1996; Pinet & Tremblay, 1995; Prave et al., 2000). Current Moho depth estimates place the Moho under the Ottawa-Bonnachere graben, which formed during Iapetan rifting, between 37 km on either side to 32 km at its center (Mereu et al., 1986).

### 1.3.3. Appalachians

Northern Appalachians east of the St. Lawrence River formed from two phases of deformation, Taconic followed by Acadian. Based on radiometric dates from ophiolites, metamorphic complexes (Whitehead et al., 1996) and biostratigraphic correlation of Iapetan sedimentary rocks (Prave et al., 2000), the Taconic orogeny was a short-lived deformational event from 485 to 440 Ma. The Taconic deformation thrust Laurentian oceanic shelf sedimentary cover onto the eastern Laurentian margin and sutured volcanic island arcs onto the continent as the east-directed (in present day coordinates) subduction drew these islands westward (Pinet & Tremblay, 1996; Castonguay & Tremblay, 2003). The deformed continental shelf deposits are seen in the Taconic Humber Zone. Between 375 and 350 Ma the Acadian terranes were sutured onto the Taconic orogen (Whitehead, 1996). The Moho depth here is estimated between ~45 and 30 km, with thinning toward the east (Li et al., 2002).

## 1.4. Summary

Geophysical studies of the Moho structure near our study area focus on either the Appalachians or the Grenville Province (Eaton et al., 2010; Cook et al., 2010). Studies focused on the Appalachian to Grenville transitional region are located far to the north or south of our study area or don't focus on resolution of the AF at the km scale (Li et al., 2002; Hynes and Rivers, 2010; Petrescu et al., 2015). The receiver grid geometry and the larger data set used in this study afford the unique opportunity to study the structure of

the Moho at the kilometer scale and to check for depth consistency between receiver functions computed from sources with varied back-azimuth directions, epicentral distances, and receivers.

## 2. Data Description

This study uses data collected from six seismic observatories, three on each side of the St. Lawrence River in Quebec, Canada. These instruments are a part of the Canadian National Seismic Network (http://www.earthquakescanada.nrcan.gc.ca/stndon/CNSN-RNSC/). All sites are equipped with similar broadband seismometers, and all have recorded seismic data continuously for the past 10-15 years. The data from these stations are publicly available, and were retrieved from the digital archives maintained by Earthquakes Canada (http://www.earthquakescanada.nrcan.gc.ca/index-en.php), a government agency tasked with seismic hazards monitoring and associated research.

Events used for RF analysis have moment magnitudes ($M_w$) greater than 5.5 recorded from years 2000 to 2013. Records of these events have clear P-wave arrivals and complete records on the vertical, north and east components. The data include only events with epicentral distances between 40° and 100° to keep P-wave paths consistent.

The total number of events processed at each receiver varied. Each site recorded between 852 and 1581 events. From the initial data set, each site had between 241 and 516 events that met the requirements for RF analysis. After narrowing the dataset to

sources within the epicentral distance range of interest, final RFs at each receiver utilized between 79 and 285 events (Figs. 3-8).

At each site, I grouped events into three back-azimuth ranges. The limits of the backazimuth (BAZ) groups are 010°-80°, 164°-200°, and 300°-350°. The number of events included in a BAZ group is 5 to 101. For each group, I constructed bin-averaged receiver functions for epicentral ranges from 40° to 100° in 10° bins with 50% overlap (i.e. each earthquake may influence two adjacent bins).

The BAZ groups were selected to be as close to parallel and oblique to the AF as possible while including as many events as possible. Passive seismic sources have an inherent geographic bias, the BAZ groups were selected to be include the maximum number of events with a continuous epicentral distance distribution.

## 3. Methods

### 3.1. Receiver Function Applications

Receiver Function (RF) analysis is a method used to resolve seismic discontinuities in horizontally layered isotropic materials (Burdick and Langston, 1977; Owens and Zandt, 1985; Ammon, 1991). Crust and upper mantle seismic discontinuities are common targets of RF studies (Burdick & Langston, 1977; Owens & Zandt, 1985; Ammon, 1991; Cassidy, 1992). The Mohorovicic discontinuity (Moho), which is the focus of this work, is a common target in RF studies due to the large difference in impedance between the crust and mantle (Burdick & Langston, 1977; Owens, 1985; Ammon, 1991; Eaton et al., 2006).

### 3.2. Basic Earthquake Physics

Distant (teleseismic) earthquakes act as a source of energy that creates compressional (P) and shear (S) waves. P waves travel at greater seismic velocities than S waves; both travel through the Earth's subsurface before being recorded at seismic observatories. Records of both P and S wave particle motion of teleseismic earthquakes typically contain both P and S polarized motion. When a P-wave passes through an interface with an impedance contrast, part of the incident energy converts into vertically (SV) polarized S-waves (Ps) (Burdick & Langston, 1977; Owens & Zandt, 1985; Ammon, 1991; Cassidy, 1992; Fig. 9).

When a P-wave incident on a seismic velocity boundary between two layers with sufficient impedance contrast produces a Ps-wave (Fig. 9), the transmitted P-wave travels at a greater seismic velocity than the converted Ps-wave. Thus, the signal of a Ps-wave from a discontinuity below the seismometer will arrive after the P-wave. The difference in arrival time between the P and the Ps-wave at the seismic station is related to the depth of the discontinuity that produced the conversion (Burdick & Langston, 1977; Owens, 1985; Ammon, 1991; Cassidy, 1992). The amplitude of the converted Ps-wave signal increases with the impedance contrast at the boundary. A combination of converted phases representing the boundaries beneath a seismic station constitutes a receiver function for it.

P and Ps wave phase arrivals are recorded on the vertical (Z) and two horizontal components (North and East) of the observing seismometer. One of the horizontal components, rotated from its original position to align with the source-to-receiver back-

azimuth, becomes the radial component. The second horizontal component, rotated with the first one and fixed at a right angle to it, becomes the transverse component. The radial component isolates the signals of the P to SV converted waves and constrains the velocity discontinuity structure under a receiver (Fig. 9). Because this study focuses on investigating velocity discontinuities and the transverse component is used to investigate anisotropy, the transverse component is ignored.

### 3.3. Receiver Function Theory

The teleseismic event records include signals from the source, path and receiver. The goal of RF analysis is to remove the source and distant path signal, isolating the P-wave and locally generated Ps signals that contain information about the seismic velocity structure near the receiver. Typically, this removal involves deconvolution, dividing the horizontal component spectrum by that of the vertical component (Burdick & Langston, 1977; Owens, 1985; Ammon, 1991; Cassidy, 1992). RF studies assume that the Ps wave should be an imperfect copy of the P-wave recorded on the horizontal components. To detect this copy, RF analysis uses a measure of similarity between the P-wave spectrum on the vertical component and the Ps-converted wave spectrum of the horizontal components. In this study, I computed RFs from the processed events using the multi-taper spectral correlation (MTC) methodology developed by Park & Levin (2000). At each seismic station, data from individual events are binned by their back-azimuths and/or epicentral distances to produce averaged RFs. The MTC methodology attempts to optimize the signal-to-noise ratio based on the coherence between vertical and horizontal

signals (expected when Ps waves look similar to converting P waves). MTC stacking amplifies the coherent P and Ps signals while minimizing the signal of incoherent noise.

Sources used in RF analysis must be teleseismic for two reasons. First, teleseismic sources ensure there is no interference between the Ps signal and the signal of primary S-waves arriving at the receiver. Primary P and S-waves must have ample distance over which to separate before the near-receiver P-to-S conversions occur. Second, incoming rays from body waves must arrive sub-vertically at the receiver. Near vertical incidence angles ensure the P-wave signal is recorded most clearly on the vertical component and the Ps-waves are recorded clearly on the radial component (Burdick & Langston, 1977; Owens, 1985; Ammon, 1991; Cassidy, 1992). Respectively, the vertical and radial components contain the highest amplitude record of P and Ps-waves. This is a result of polarization of particle motion for P-waves parallel to the plane of the ray and Ps-waves perpendicular to the ray.

Based on the difference in their velocities and their expected angles of incidence, primary P and S-waves produced by events with epicentral distances greater than approximately 30° fulfill both conditions, preserving clear Ps records (Cassidy, 1992). However, offsets of greater than 40° produce clearer signals; thus, 40° is the minimum epicentral distance used in this study.

### 3.4. Study Area Description

This study uses a grid of seismometers and multiple epicentral RFs computed from their radial components to produce a depth map of the Moho below a section of the

Saint Lawrence River, Quebec, Canada. Epicentral RFs represent 2D time delay profiles along the stacked events' back azimuth direction (Fig. 10). RFs are binned first by a relatively narrow back-azimuth range, then by epicentral distance (Fig. 10). Back-azimuthal windows for the epicentral RFs range from 10° to 70°, depending on their data density. In a given back-azimuth range, events originating within 10° of epicentral distance of each other are combined, from distances of 40° to 100°. Rays from nearer events arrive at shallower incidence angles (Burdick & Langston, 1977), and travel longer paths from seismic boundaries than those with farther offsets (Fig. 10). The effect is similar to the normal move-out in seismic reflection data, but reversed. Due to the geometry of P and S wave ray paths involved (Fig. 10a) for a seismic boundary at depth, RFs with shorter epicentral distances will have greater time delays for Ps conversions at the same depth than those produced from sources at greater epicentral distances.

### 3.5. Receiver Function Modeling

If the material under a receiver is horizontally layered and isotropic, all of the energy from the P-to-S conversion should be polarized as an SV-wave. In this scenario, the event would only be recorded on the vertical and radial components. The transverse component would record no signal. However, this is almost never the case as most materials sampled by the events are not completely isotropic and boundaries are rarely horizontal (Cassidy, 1992; Park & Levin, 1997). This study only considers RFs produced from radial components to image discontinuity structures.

The seismograms used for RF analysis underwent quality control individually on a visual basis to meet the criteria for RF analysis. First, the records must contain a signal that is distinct from the noise. Furthermore, each of the three components must have recorded a clear primary P-wave arrival. On seismograms with obvious P-waves, I selected the P-wave arrival times and discarded time series with an unclear P-wave. Because the P and Ps waves were of interest, the time series were cut into 650-second records. The 150 seconds before the P-wave arrival allowed pre-event noise analysis, whereas the remaining 500 seconds are the part of the record that contains P-to-S conversion signals. The three-component records are then filtered to remove noise at frequencies below 0.02 Hz.

The time delays of Moho-induced Ps phases were interpreted in epicentral RFs. Observed delay times were converted to depth using a modified whole-Earth 1D velocity model in the TauP Toolkit (Crotwell et al., 1999). The crustal P and S velocity ($V_p$, 6.45 km/s and $V_s$, 3.69 km/s, respectively) intervals were modified from the velocity profiles generated by Tesauro et al. (2014; Fig. 11). The model velocity structure below the Moho was taken from the ak135 whole-Earth model (Kennet et al., 1995; Fig. 12). The crustal thickness of the velocity model was selected based on the maximum interpreted Moho time delay in the RFs used in this study. The Moho depth imposed in the modified TauP model were calculated using the thickness equation described below (Gurrola & Minster, 1998):

Eq. 1:
$$H_{thickness} = \frac{t_{Ps}}{\sqrt{\left(\frac{1}{V_S^2}\right) - p^2} - \sqrt{\left(\frac{1}{V_S^2}\right) - p^2}}$$

Where $H$ is crustal thickness, $t_{ps}$ is the maximum time delay used as input, $V_p$ and $V_s$ are the average crustal P and S wave velocities used in the model, and p is the ray parameter at an epicentral distance of 70°. A maximum crustal thickness of 50 km is imposed on the model based on this formula. In the actual model used as input for the TauP calculations, the crustal $V_p$ and $V_s$ values are increased one ten thousandth of a km/s per km of depth. This modification from initially constant values is necessary to produce outputs with the TauP software, which accommodate the variable time delays from the interpreted Moho Ps phase in the RFs.

P and Ps ray paths pierce points (Fig. 10) are modeled to produce time delays, depths, and coordinates for a range of depths, from the base of the crust to the Earth's surface. Ps-wave pierce points are computed for interfaces placed every 1 km in the crust, from the surface to the Moho, and predicted times are matched with the delay times of the Moho associated Ps phase from the RFs. The TauP modeled time delays that are closest to the observed delays are used to convert these observed delays to depth. To preserve the spatial uniqueness and consistency of individual epicentral RFs, the depths are associated with the coordinates of the Moho-converted Ps-wave at 50 km. Based on the epicentral RF interpretations, modeled depths are used with the back-azimuth and epicentral distances to calculate the latitude and longitude coordinates of Ps phase conversions at the base of the crust (Figs. 10 & 13). The Moho is mapped on each 2D profile once depths and coordinates are constrained from observational and modeled data (Fig. 14). Finally, a time delay map of the Moho is constructed from the interpolation of the RF profiles (Fig. 15), which is later used to convert the RF time-delays to depth.

RF phases interpreted as the Moho-generated Ps must meet certain criteria in the 1 Hz epicentral RF. The polarity of the phase must be positive to be consistent with an increase in velocity with depth across the boundary. Additionally, it should be associated with delay times between 4.5-6.3 seconds. Delay times earlier that 4.5 s indicate Moho depths less than 35 km and later than 6.3 s would indicate depths greater than 50 km. There is no evidence from previous studies that the Moho here should exceed depths of 50 km or be shallower than 35 km (the global crustal average). The interpreted phase should also be continuous across all distance bins for a given profile. Time delays for a phase should decrease with increased epicentral distance but may not depending on the geometry and presence of other seismic discontinuities.

Before final interpretation of the epicentral RF profiles, I consulted the back-azimuthal RFs. Back-azimuthal RFs are used as a preliminary step to identify complex phases that may correspond with the Moho and their approximate arrival times. After phases of interest are identified from the back-azimuthal and 1 Hz epicentral RFs, the epicentral RFs are revisited at 2 Hz to determine if higher frequency noise contributes to complex move-out geometry and the presence of double pulses. RFs are ignored in the final interpretation if there is no obvious Ps phase associated with the Moho, the move-out geometry is complex and cannot be clarified in the 2 Hz epicentral profiles, or there are multiple pulses associated with the Moho with no dominant phase that can be interpreted on either the 1 or 2 Hz profiles.

Once the Moho associated Ps phase is identified based on the criteria above, the time-delays of that phase are selected. The time-delays associated with the maximum value of that phase span up to .23 s. To select one time delay the mean value of the

maximum amplitude is used to estimate depth. Using the mean value of the maximum amplitude introduces potential error of up to +/- 1 km (based on Eq. 1) for Moho depth estimates depending on the broadness of the maximum.

The $V_p/V_s$ ratio used in this study (1.746, e.g. Tesauro et al., 2014) was the minimum determined by studies on the $V_p/V_s$ structure of this region. Alternatively using the maximum $V_p/V_s$ determined for this region of ~1.87, the depth estimates of discontinuities under these receivers shallow by ~5 km.

The other possible source of error is introduced during interpretation of the lower frequency (1 Hz) RFs. When the 2 Hz RFs are consulted the primary phase interpreted as the Moho in the 1 Hz RFs often breaks down into multiple positive phases that can be interpreted in individual RF profiles and miscorrelation of these phases could result in more variable depth estimates.

## 4. Results

In this section, I describe the epicentral RFs at each site. RF profiles at each site use maximum frequencies of 1Hz. Sites A11, A16 and A21 are situated on Appalachian Taconic Humber zone on the southeastern bank of the St. Lawrence River; sites A54, A61 and A64 are located across the river and Appalachian Front (AF) on the Grenville terrane. The receivers are distributed evenly between the southeastern and northwestern banks of the St. Lawrence River. RF profiles oriented along azimuths near perpendicular (NW), near parallel (NE) or oblique (S) to the AF (Fig. 13) are available for each site. Each profile has the average azimuth of the event back-azimuths. I describe the RF

profiles and interpret one of the phases as the Moho (Figs. 16-21). The time delays associated with the phase interpreted as the Moho are converted to depth, yielding time delay and depth maps from the interpreted RFs (Fig. 15).

### 4.1. Site A11

In the back-azimuthal sweeps (Fig. 16) there is a high amplitude positive phase with arrival times appropriate for interpretation as the P-to-S converted Moho phase (5-6 s) in the 300°-350° back-azimuth range. Comparison of the RF profiles at 1 Hz (Fig. 17) and 2 Hz (Fig. 18) indicate the Moho is complex under this site. At lower frequencies the Moho induced Ps phase appears as a single pulse, whereas at higher frequencies the individual pulse separates into at least two lower amplitude positive phases. The resultant time delays in 1 Hz RFs may represent a combination of multiple Ps phases at 2 Hz.

#### 4.1.1. Epicentral Receiver Function, Baz 300°-350°

The Moho is only interpreted in the NW-SE RF profile at this site. These RFs are composed of events with back-azimuth ranges and epicentral distances between 300°-350° and 40°-100°, respectively (Fig. 17a & 18a). The profile has three strong positive amplitudes at 0-10 s of delay time. The positive high amplitude phase of interest arrives between 5.5 and 6.5 s. Between the second and third positive phases (6.5-8 s) the only strong negative amplitude appears.

The second positive pulse arrival at 5.5-6.5 s is the most prominent of the three

positive amplitudes. It is interpreted as the Moho induced phase arrival because it arrives at time delays that can be associated with the Moho Ps phase. For the most distant sources the time delay of this phase increases somewhat with epicentral distance, indicating the boundary may deepen closer to the receiver.

The irregular move-out observed in the 1 Hz profiles may be a result of the combination of multiple higher frequency Ps phases. The 2 Hz profile computed from the same data shows a clear primary positive phase with delay times consistent with the 1 Hz interpretations and a second, smaller positive pulse that arrives after it and begins to merge with the primary phase between epicentral distances of 90° and 100°. The positive polarity of the phase interpreted as the Moho indicates an increase in velocity with increased depth, consistent with the velocity change expected from the crust-to-mantle transition. Depth estimates from this phases time delays range are 44-50 km, indicating possible increased Moho depth near the receiver.

**4.2. Site A16**

The back-azimuthal sweeps (Fig. 19) at this site indicate a clear positive phase that arrives in time ranges acceptable for interpretation as the Moho phase from all directions. All three epicentral profiles are interpreted at this receiver. The 1 Hz epicentral RF profiles produce a single strong clear positive pulse. The pulse interpreted as the Moho at 1 Hz (Fig. 20) divides into multiple pulses below this site; however, at 2 Hz (Fig. 21) the highest amplitude phase arrives at similar times as in the 1 Hz RFs.

### 4.2.1. Epicentral Receiver Function, Baz 300°-350°

The NW-SE epicentral profile is computed for events in back-azimuth and epicentral distance ranges of 300°-350° and 40°-100°, respectively. A strong positive phase arrival is at 4-6.5 s. A double pulse with 2 large local maxima is present in this time delay window for RFs of 40°-50° of epicentral distance. The 2 Hz RFs exhibit a doublet, and sometimes a triplet, of local maxima across all bins. This amplitude becomes more coherent for events with distances of 60°-100°, and its delay time decreases with increased epicentral distance, as expected for a horizontal converting boundary.

The positive phase arrival at 4-6.5 s indicates a downward increase in seismic velocity across the interface producing these phases. Time delays associated with this discontinuity are appropriate for the expected delay associated with the Moho and produce depth estimates between 48-50 km. The double pulse between 40°-60° epicentral distance could be a result of multiple increases in seismic velocity across the interface that produced this signal. The 2 Hz epicentral RFs support this interpretation.

### 4.2.2 Epicentral Receiver Function, Baz 015°-075°

The NE-SW epicentral RFs are computed for sources with back-azimuths of 015°-075° and epicentral distances of 50°-100° at 1 Hz (Fig. 20b). The largest coherent positive amplitude arrives at 4-6.5 s and is followed by a coupled small negative and small positive phase at 6.5-7 s in the 50°-70° bins. The second small positive signal

begins to merge with the coherent 4-6 s signal between epicentral distances of 70°-100°.

The only phase with a consistent and interpretable signal arrives from 4 to 6.5 s. I interpret it as the Moho phase due to its time delays and the strength and coherence of its signal. The peak of this phase has variable delay times; its arrival times become earlier from 50°-70°, then later from 70°-90°, finally arriving at their earliest delay time at 100° epicentral distance. In the 2 Hz RFs (Fig. 21b) the strength of the phases interpreted as the Moho signals decreases, but their time delays become more consistent. At epicentral distances of 80°-100° lower amplitude phases before and after the phase interpreted as the Moho may influence the observed arrival times in the 1 Hz RFs. The combinations of the phases observed in the higher frequency RFs make them more variable and produce an unexpected move-out in the 1 Hz profile. The positive phase arriving in this time interval indicates an increase in seismic velocity with depth. Depth estimates of the Moho phase range from 40 to 45 km for this profile.

### 4.2.3. Epicentral Receiver Function, Baz 164°-195°

The N-S profile utilizes back-azimuths of 164°-195° and epicentral distances of 40°-90° at 1 Hz (Fig. 20c). The maximum amplitude signal arrives between 4 and 6 s; this phase is consistent and coherent. Following the maximum positive pulse, a weak negatively polarized phase occurs between 6 and 7.5 s that becomes increasingly broad at greater epicentral distances.

The Moho phase is likely associated with the 4-6 s pulse delay times. This pulse has a slight concave down geometry in the RF profile. From 40° to 70° of epicentral

distance its arrival time becomes progressively earlier; at 80°-90° the arrival times of the maximum become later than in each previous bin. At 2 Hz (Fig. 21c) the pulse interpreted as the Moho arrives at similar delay times as those observed at 1 Hz. The concave geometry of this phase is likely an artifact of the data exemplified in the 2 Hz profile, but may indicate slight relief in the geometry of the Moho under the Appalachians. Depth estimates based on interpretation of this phase as the Moho vary from 43 to 44.5 km.

### 4.3. Site A21

Back-azimuthal sweeps (Fig. 22) confirm clear signals likely produced at the Moho from BAZ directions of 120°-270° and 300°-350°. Identification of a Moho Ps phase is unclear from 000°-090°; for this reason the NE-SW epicentral profile (Figs. 23b & 24b) is left out of final interpretations. The NW-SE profile filtered at 1 Hz (Fig. 23a) and 2 Hz (Fig. 24a) shows a complex crust-to-mantle transition with a double positive phase arrival in the RFs.

#### 4.3.1. Epicentral Receiver Function, Baz 300°-350°

The NW-SE profile utilizes events with back-azimuths of 300°-350° over epicentral distances of 40°-100°. Two high-amplitude very coherent positive phases with delay times of 4-7 s follow a weak negative-phase arrival. The first positive peak's arrival

time stays consistent over all epicentral distances and arrives at 4-5 s. In contrast, the second positive peak is larger, arrives between 5-7 s, and gets progressively earlier with increasing epicentral distance. The second phase arrival at 5-7 s is interpreted as the Moho phase because of the strength of its signal. A coherent negative signal in 7-9 s range follows.

The strong positive signal that arrives at 4-5 s coupled with the Moho signal interpreted at 5-7 s may indicate the presence a thin layer of material above the Moho. The move-out of the Moho amplitude at 5-7 s is consistent with that of Ps phases generated at a horizontal boundary. The negative pulse that arrives immediately after this phase indicates a decrease in seismic velocity with depth. The velocity structure here is a two-step increase in velocity with increased depth, once in the lower crust and again across the crust-mantle transition. The phases observed in the 2 Hz RFs are consistent with those in the lower frequency (1 Hz, Fig. 23) profiles. However, based on the 2 Hz RFs, the layer above the Moho may increase in velocity from mid to lower crust, and then produce a slight decrease in velocity before increasing again across the Moho. Depth estimates of the phase interpreted as the Moho (5-7 s) on this profile are 47-49 km.

### 4.3.2. Epicentral Receiver Function, Baz 170°-200°

The N-S profile utilizes events with back-azimuths of 170°-200°and epicentral distances of 40°-80°. The RF maximum arrives between 4.5 and 6.5 s, followed by a large amplitude negative minimum. The 2 Hz filtered epicentral profile is less coherent but still produces only a single positive phase within the same time range discussed

above. Its delay time becomes smaller with increasing epicentral distance.

The delay times associated with the positive amplitude produce the expected move-out geometry for a near horizontal boundary that produces Ps conversions. Because the 4-6.5 s amplitude is the most significant, its delay times are consistent with Ps phases produced at a Moho. The positive phase interpreted as the Moho (4.5-6.5 s) indicates a velocity change from slow to fast material with increased depth. Depth estimates along this profile range from 41.5 to 44 km.

### 4.4. Site A54

Data from this site display significant directional variability (Figure 25). Delays of target phases likely associated with the Moho change systematically with BAZ, suggesting a dipping interface. All epicentral profiles produce a single positive phase interpreted as the Moho at 1 Hz (Fig. 26). I consulted RFs produced at 2 Hz (Fig. 27) when move-out of the Ps phase has an unexpected geometry.

#### 4.4.1. Epicentral Receiver Function, Baz 300°-350°

The back-azimuth range for the NW-SE profile was 300°-350°; this range produced RFs at epicentral distances of 60°-100°. The only coherent positive amplitude in this epicentral RF profile arrives at 5-6 s. Its arrival time decreases with increased epicentral distance. A negatively polarized phase arrives at 7-8 s.

The only coherent positive phase interpretable as the Moho is the 5-6 s arrival.

The positive phase here indicates an increase in seismic velocity from crust to mantle. It's immediately followed by a negative phase indicating a decrease in seismic velocity with increasing depth within the upper mantle. Arrival times associated with the positive phase are consistent with Ps phase delays from Moho conversions. Depth estimates along this profile range from 49 to 50 km.

### 4.4.2. Epicentral Receiver Function, Baz 030°-050°

The NE-SW profile utilizes events with back-azimuths of 030°-050° and epicentral distances of 70°-100°. A large positive and coherent maximum phase arrives at 4.5-6 s. A weak negative phase has delay times of 6-7 s.

The 4.5-6 s delay time is the only phase interpretable as the Moho. Its amplitude is the maximum for the entire RF. This phase has the opposite move-out with respect to that expected for a Ps-wave converted at a horizontal interface. The 2 Hz signals (Fig. 27) indicate the abnormal move-out of the phase observed in the 1 Hz RFs (Fig. 26) is the result of the confluence of two higher frequency signals. The positive phase at 4.5-6 s indicates a change from seismically slow to seismically fast material with increasing depth. This is consistent with the interpretation of the 4.5-6 s phase as the Moho derived Ps-wave arrival. Moho depth estimates along this profile are 40-45 km.

### 4.4.3. Epicentral Receiver Function, Baz 180°-190°

The N-S epicentral RF profile utilizes events in the back-azimuth range 180°-190°

and epicentral distances of 50°-90°. A high amplitude positive phase arrives between 4.5-6 s; a coherent negatively polarized phase arrives at 6-7 s. The positive phases' delay times become earlier with increasing epicentral distance.

I interpret the 4.5-6 s positive polarity as the Moho in this RF profile. The polarity change from negative phase observed before the positive Moho phase is consistent with slow to fast velocity transition from crust to mantle. The negative phase observed following the arrival of the Moho phase indicates a transition from higher to lower seismic velocities in the upper mantle. The time delays of the positive phase decrease with increasing epicentral distance, indicating a near horizontal crust-mantle transition along strike of this profile. Moho depth estimates along this profile are 42.5-43 km.

### 4.5. Site A61

The back-azimuth gather for this station (Fig. 28) displays a systematic variation of the likely Moho converted Ps phase delay times, suggesting some amount of dip of this interface. Investigation of the 1 Hz (Fig. 29) and 2 Hz (Fig. 30) RF profiles oriented NW-SE and NE-SW from this receiver may indicate a complex crust to mantle transition involving a thin layer of material emplaced above the Moho (Fig. 29a, 29b, 30a, & 30b).

#### 4.5.1. Epicentral Receiver Function, Baz 310°-340°

The NW-SE profile utilizes source back-azimuths of 310°-340° and epicentral distances of 40°-100°. A positive polarity doublet arrives between 3.5 and 6.5 s; the

maximum positive phase of the doublet arrives from 5 to 6.5 s.

The 5-6.5 s phase has the highest amplitude in every data bin; I picked it as the Moho phase. The time delays from this phase produce a concave-up geometry. The positive doublet observed between 3.5-6.5s in the 1 and 2 Hz RF profiles may indicate a crustal layer above the Moho that produces a two-step increase in seismic velocity with increasing depth. First seismic velocity increases within the lower crust and again at the crust-mantle transition. Moho depth estimates along this profile vary between 47.5 and 50 km.

### 4.5.2. Epicentral Receiver Function, Baz 020°-080°

The NE-SW profile utilizes source back-azimuths of 020°-080°and epicentral distances of 40°-100°. A high-amplitude positive polarity is present at 4.25-6 s of delay time. This signal becomes less coherent with increased epicentral distance and bifurcates at 60°-100°. The signal from 6-10 s is incoherent and mixed between positive and negative polarities.

I interpret the 4.25-6 s phase as the Moho. Its time delay increases with epicentral distance from 40° to 70° but develops the move-out of a horizontal boundary from 70° to 100°. In the 2 Hz filtered RFs (Fig. 30b) the doublet observed at 60°-100° epicentral distance is pronounced in all epicentral distance bins. The double pulse may indicate a complex crust-mantle transition due to a thin layer of material, seismically faster than the rest of the crust, emplaced above the Moho. Moho depth estimates vary along this profile from 44 to 50 km.

### 4.5.3. Epicentral Receiver Function, Baz 170°-190°

The N-S profile utilizes source back-azimuths of 170°-190° and epicentral distances of 40°-100°. It shows a coherent negative phase whose signal strength decreases with increase offset from the receiver at 3.5-5.5 s coupled with a large coherent positive amplitude arrival at 5.5-6.5 s. From 6.5 to 10 s a 0.5 s wide negative low amplitude is coupled with a weak positive signal of the same time-width followed by another low amplitude negative signal.

I interpret the 5.5-6.5 s pulse as the Moho induced Ps phase. The 5.5-6.5 s signal is clear and positive; its time delays are consistent across epicentral distance bins. Time delays that do not vary in the RF significantly may indicate a boundary that deepens with proximity to the receiver. Along this profile, Moho depth estimates vary from 47 to 50 km.

## 4.6. Site A64

The back-azimuth gather (Fig. 31) at this site shows variation in Moho depth with direction. The NE-SW and N-S epicentral profiles filtered at 1 Hz and 2 Hz exhibit a single high-amplitude arrival. I ignore the NW-SE profile in the 1 Hz interpretations (Fig. 32) of the Moho; this is the only case where I used the 2 Hz (Fig. 33) Moho profile for the interpretation.

### 4.6.1. Epicentral Receiver Function, Baz 300°-350°

The NW-SE profile utilizes from events with back-azimuths of 310°-340°and epicentral distances of 50°-100°. A single high-amplitude positive pulse in the 1 Hz profile (Fig. 32a) for 50°-70° arrives at 4-7 s; it bifurcates into two positively polarized pulses for 80°-100°, making it difficult to interpret. In the 2 Hz profile (Fig. 33a) two distinct positive pulses are present in all epicentral distance bins; the first arrives at 4.5-5.5 s and the second at 5.5-6 s. I interpret the second pulse as the Moho induced Ps phase. In both 1 Hz and 2 Hz RFs, a negative pulse immediately follows the later Ps phase arrival.

The double pulse observed in RFs computed from more distant events at 1 Hz and all bins at 2 Hz may indicate the presence of a thin layer of material emplaced in the lower crust. Based on the RFs, the 4.5-5.5 s positive pulse indicates an increase in velocity from the mid to lower crust. The 5.5-6 s positive phase indicates a second velocity increase across the crust to mantle transition. The negative polarity following the phase interpreted as the Moho indicates a downward shift in seismic velocity from fast to slow in the upper mantle.

### 4.6.2. Epicentral Receiver Function, Baz 010°-065°

The NE-SW profile utilizes events with back-azimuths of 010°-065° and epicentral distances of 40°-90°, respectively. Between 4-5.5 s the positive maximum of the time series arrives. I interpret the 4-5.5 s positive phase as the Moho. It is the highest

amplitude phase in all data bins. This phase produces a time delay move-out consistent with a near horizontal interface. The positive phase interpreted as the Moho indicates the appropriate seismic velocity change from slow velocity above the discontinuity to fast below it. It is followed by a negative amplitude pulse that indicates a shift from seismically slow material below the interface to fast above it, likely located within the upper mantle. Moho depth estimates along this profile vary from 37.5 to 38.5 km.

### 4.6.3. Epicentral Receiver Function, Baz 170°-190°

The N-S profile utilizes sources with back-azimuths of 170°-190° and epicentral distances of 50°-90°. The RFs' maximum positive phase arrives at 4-5.5 s, then a weak but consistent negative phase arrives at 5.5-6.5 s.

I interpret the 4-5.5s amplitude arrival as the Moho related phase. It is the maximum observed amplitude in every data bin and produces the expected move-out of a real, near-horizontal boundary. Additionally, the negatively polarized arrival following this phase indicates a decrease in seismic velocity with depth consistent with the interpretation of this phase as the Moho. Along this profile Moho depth varies from 36.5 to 37.5 km.

## 4.7. Results Summary: Figs. 34, 35 & 36

The time delay and depth maps plotted using modeled Ps pierce points show significant relief and complexity in the crust to mantle transition in this study area (Figs.

15, 34, & 35). Using the modified ak135 velocity model and interpreted RFs with simple geometries (i.e. expected moveouts with single high amplitude positive pulses) I find that the Moho depth varies from 37 to 50 km. Individual sites show depth changes on the order of 5-10 km between directional RF profiles. Between some stations, depths can change by as much as 12 km compared to depth estimates of adjacent receivers. Additionally, RFs at sites A21, A61 and A64 exhibit multiple high-amplitude positive phases that may indicate a layer of material emplaced above the Moho.

Sites A21 produces depth variations of 8 km from the maximum depth of 50 km observed in the NW-SE profile to a minimum depth of 42 km in the N-S profile (Figs. 23, 24, & 34). The two profiles at site A21 vary by up to 10 km as well; the NW-SE profile produces 50 km Moho depth estimates while the N-S profile shows a minimum of 41.5 km. Similarly, site A16 indicates variability of up to 7 km between the NW-SE profile where the maximum site depth is 50 km is observed, and the N-S profile (Figs. 20c & 34) with intermediate site depths of 43 km. The A16 profiles show 10 km of relief between the NW-SE profile (50 km) and the NE-SW profile where the minimum site depth is 40 km (Figs. 20a, 20b, & 34). Profiles from Site A54 produce 7.5 km of Moho depth variation. The maximum Moho depth of 50 km occurs on the NW-SE profile; the Moho depths on the NE-SW profile and N-S profile are largely consistent, with observed depths of 42.5-45 km. Site A61 produces consistently deep estimates of ~50 km while the Moho at site A64 is significantly shallower at 37-40 km (Figs. 32, 33, & 34).

The NW-SE profiles at each site produce similar depth estimates of 47-50 km. These profiles are consistent between sites on both sides of the AF; however, they are deeper than all other profiles except at site A61, which consistently yields the deepest

Moho depth estimates (50 km in all profiles). This consistent directional variability may indicate a dipping Moho interface.

Two cross sections A-A' and B-B' (Figs. 35 & 36) illustrate Moho relief along and across the AF. The A-A' cross section is perpendicular to the AF (NW-SE) and uses projections from NW-SE and N-S oriented profiles from sites A61 and A16 (Figs. 34, 35 & 36a). The B-B' cross section is parallel to the AF (NE-SW) and utilizes the NE-SW profiles at sites A54, A61, and A64 that lie on Grenville material (Figs. 34, 35 & 36b). The B-B' cross section shows slight crustal thickening of ~5 km from its SW end to its center, followed by significant thinning to the NE from 50 km to ~40 km; the Moho structure parallel to the AF is asymmetrical, concave upward, and shallowest to the NE. The A-A' cross-section shows a general trend of crustal thinning from NW to SE across the AF.

## 5. Discussion

### 5.1. Previous studies

The crust-mantle transition has been a target of several geophysical refraction, reflection and passive geophysical studies under the Grenville province and Appalachian mountains. Studies of NE North America have produced variable results and success in resolving the Moho (Eaton et al., 2006; Carr et al., 2000; White et al., 2000, Mereu et al., 1986; Rondenay et al, 2000; Taylor & Toksoz, 1982; Musacchio et al., 1997; Li et al., 2002; Hughes & Luetgert, 1991). The Grenvillian Moho has been the subject of more study recently, both to the west in Quebec and southwest in New York, as a result of the

Lithoprobe, MOMA, and COCORP projects (Eaton et al., 2006; Carr et al., 2000; White et al., 2000, Mereu et al., 1986; Rondenay et al, 2000, Li et al., 2002). Geophysical estimations of the Moho depth in the Grenville province vary from 50 km to 35 km with general shallowing eastward away from the Grenville front (GF). Lower crustal deformation produced deep-reaching faults up to 20 km into the crust as a result of thick-skinned deformation (White et al., 2000; Carr et al., 2000). Additionally, previous studies have shown that the Moho under the Grenville is not always easily observed. Seismic resolution of the crust-mantle boundary degrades most often due to attenuation and low impedance contrast resulting from high-velocity lower crustal material overlying the Moho (Carr et al., 2000).

The Moho under the AF and New England Appalachians have been the target of multiple studies as well; they focus on the boundary ~200 km south of the lower St. Lawrence river (Mussachio et al., 1997; Li et al.,2002; Taylor & Toksoz, 1982). Studies disagree about how the Moho structure changes across and within the Appalachians. Initial study by Taylor & Toksoz (1982) proposed crustal thickening across the AF, from 36 km thick Grenville crust to 40 km under the Appalachians. However, Mussachio et al. (1997) proposed crustal thinning from west to east across the AF based on an O-NYNEX refraction profile; they estimated the Moho depth at 45 km under the Grenville province and shallowing to 35 km under the Appalachians. This interpretation is in agreement with Moho depth estimates proposed by Hughes & Leutgart (1991), who also used wide-angle refraction methodology targeting the Moho across the AF in a very similar region. However, Li et al. (2002), using RFs, observed a more variable Moho across the AF. Their transect crosses the AF to the SW of the O-NYNEX profile; here they estimated the

Moho depth at 50 km under the AF, shallowing to ~45 km just to the east and finally shallowing further to ~32 km near the Atlantic coast of Massachusetts.

### 5.2. Moho Relief

Based on the results of RF analysis and time-to-depth conversion, I interpret at least as much variability in Moho topography under this region as in the studies discussed above (Taylor & Toskoz, 1982; Hughes & Leutgart, 1991; Mussachio et al., 1997; Li et al., 2002; Fig. 34); notably, these changes in Moho topography happen over a much smaller region. Depth estimates from the RF analysis under the St. Lawrence River show a complex crust-to-mantle transition. A generally consistent Moho depth of 43-50 km occurs below the receivers located in the SW region of the study area (Figs. 17, 18, 20, 21, 26, 27, 29, 30, & 34). Crustal thinning appears to occur in the NE region of the study area to minimum Moho depths of ~35 km. The NE-SW profile at site A16 produces Moho depth estimates of ~40 km (Figs. 20, 21 & 34) in approximate agreement with the profiles at site A64 where the Moho depth varies from 35 to 40 km. The Moho depth of ~40 km estimated from the southern profile at site A21 (Figs. 23c, 24c, & 34) is also in agreement with the A16 and A64 profiles (Figs. 20, 21, 32, 33, & 34). However, A21 produces a notable outlier (Figs. 23a, 24a, & 34) when compared to results from nearby profiles. The NW-SE profile at site A21 (Figs. 23a & 24a) shows a clear high amplitude Ps phase with the move-out expected from a real, horizontal boundary that produces depth estimates 10 km greater than that of the profiles discussed at sites A16 and A64 (Figs. 20b, 21b, 32c, 33c, 34, & 35).

The presence of large ~10 km variations in Moho depth over lateral extents of less than 20 km is explainable in three ways. Either the Moho is offset, there is a locally variable high-velocity layer in lower crust, or the crust to mantle transition is complex layered and potentially non-discrete boundary. The first scenario requires deep-reaching shear zones oriented oblique (WNW to ESE) to the trend of regional structures (NE to SW) in this region (i.e. Logan's fault; Figs. 34 & 35). None of the established faults in this region are known to offset the Moho abruptly; thus, I deem it less likely than the other explanations.

### 5.3. Thin Layer

The depth estimates on the N-S and NE-SW RF profiles at site A64 (Fig. 22b & 22c), the NE-SW profile at Site A16 (Figs. 20b & 21b) and the N-S profile at Site A21, all of which range from ~35 to 40 km, are in general agreement. Each of the phases interpreted in these RFs (Figs. 23b, 23c, 24b & 24c) exhibits a single simple pulse interpreted as the Moho. The depth estimates from these profiles are difficult to reconcile with RFs both at the same sites and with the remaining sites, where Moho depth estimates reach 50 km.

The RF profiles with double Ps phases at sites A21 (Figs. 23a & 24a), A61 (Figs. 29a, 29b, 30a, & 30b) and A64 (Figs. 32a & 33a), in the NW region of the study area present a possible explanation for variable RF depth estimates. The profile in Fig. 19a shows a double pulse that indicates an increase in velocity in the lower crust, above the phase interpreted as the Moho. This shallower discontinuity is more consistent with the

phases interpreted in the adjacent A64 profiles with single pulses (Figs. 32b, 32c, 33b, 33c, 34 & 35). The double pulse exhibited at RF profiles at site A21 (Figs. 23a & 24a), A61 (Figs. 29a, 29b, 30a, & 30b) and A64 (Figs. 32a & 33a) may indicate a layer of seismically fast material (relative to average crustal velocities) above the mantle.

The lower crustal layer of material would be of variable thickness and range from ~10-20 km thick. It is possible that the profiles with shallow single pulses correlate more closely with the positive Ps phases produced at the top of the lower-crustal layer. The profiles that produce deep (~45-50 km) Moho depth estimates correlate with the later arriving phase observed in the profiles that exhibit positive doublets.

The thin layer of material above the Moho may be local to the NW region of the study area. The apparent depth variation in the Moho observed in the rest of the region is explainable by a dipping Moho boundary. This layer of material could have been emplaced either during the widespread magmatism related to Iapetan rift and drift or arc volcanism during the Taconic orogeny.

The proposed layer of material results in a locally thicker crust that should cause topographic relief where the layer is present. If the lower crustal layer is seismically faster (and thus, denser) than the rest of the lower crust in this region, there should also be a gravitational anomaly associated with it. However, the topography of the study area does not show a significant change to locally accommodate a much thicker lower crust. Bouguer gravity anomaly maps (Pinet et al., 2010) do not show a significant anomaly anywhere in the study region. Thus, isostatic compensation deeper within the lithosphere may account for the lack of topographic relief.

### 5.4. Complex Crust-to-Mantle Transition Zone

An alternative explanation is that the lower crust consists of multiple layers with only two visible seismic boundaries in the NW region, where the impedance contrasts between the Moho, the lower crustal layers and the overlying crust are significant enough to produce two Ps conversions. At the profiles that show a single Ps converted phase associated with the Moho, depth estimates vary by up to 15 km. The profiles that show a deep Moho discontinuity would be the result of a high impedance contrast from mantle to lower crust followed by a complex and gradual velocity decrease within the lower crust that is not conducive to Ps conversions. Where Moho depth estimates are shallower (~35-40 km) and interpreted based on a single pulse, the mantle may initially transition gradually to the crust before reaching impedance contrasts at shallower depths sufficient to produce Ps conversions within the lower crust.

All scenarios mentioned above imply that supercontinent assembly and dispersal events have long lived effects on the properties of the lower crust and Moho.

## 6. Conclusions

Like previous geophysical studies of the Appalachian and Grenville provinces, this study encountered difficulty in consistently resolving a single and simple Moho boundary in this region. Although orogenic processes have not deformed the region over the last 350 million years, the relict complexity and active geologic history of the region

suggest that a complex crust-to-mantle transition is likely. The possible implications of the RF analysis conducted in this study are:

1. Multiple shear zones that offset the Moho
2. A complex velocity structure under the receivers involving a seismically fast lower crustal layer.

or

3. A complex crust-to-mantle transition zone with variable relative velocity changes

The first possibility is unlikely. The orientations of the shear zones that would have to be present to offset the Moho would be roughly orthogonal to the strike of the mapped faults in this region. To produce the Moho depth variations from these RF depth estimates the shear zones would have had to reach up to 50 km below the surface causing offsets of 10-15 km. This deformation would presumably have occurred during Appalachian, Iapetan and/or Grenville deformation.

The second scenario is more likely than mantle offset. A layer of material could have been emplaced above the Moho, most likely during Iapetan rifting as an igneous intrusion of mantle-derived melt, or else during Appalachian subduction and arc volcanism. This scenario could explain the difficulty in resolving the crust-mantle boundary in this region. RFs that produce double Ps phases are strong evidence for a step increase in velocity from the crust to the mantle. In RFs that produce single Moho Ps phases, this layer could still be present but not resolvable if the impedance contrast between either the lower crustal layer and the Moho or the crust above this layer are insufficient to produce multiple Ps conversions. However, the likely topographic and gravitational expression of the presence of this layer are not present.

The third scenario is the most likely. A complex, layered crust-to-mantle transition would cause double pulses at sites with sufficient impedance contrast between layers of different velocity to produce two Ps conversions. Where single pulses are present at depths greater than 45 km, the impedance contrast at the Moho is significant, and the layers above it are too thin to produce observable Ps conversions, resulting in a gradational velocity change at the base of the crust. Where single pulses are present at depth estimates of less than 40 km, the velocity decrease from mantle to crust is gradual at greater depths and most significant at the top of the complex transition zone.

## 7. Bibliography


Alkok, F.J. (1945), Logan's Fault, *The Royal Astron. Soc. of Can., 39, 213-216.*

Ammon, C. J. (1991), The isolation of receiver effects from teleseismic P waveforms, *Bull. Seism. Soc. Am.,* 81, 2504-2510.

Cassidy, J.F. (1992), Numerical experiments in broadband receiver functions analysis, *Bull. Seism. Soc. Am.*, 82, 3, 1453-1474.

Carr, S.D., Easton, R.M., Jamieson, R.A., Culshaw, N.G. (2000), Geologic transect across the Grenville orogen of Ontario and New York. *Can. J. Earth Sci.,* 27, 193–216.

Castonguay, S., Tremblay, A. (2003), Tectonic evolution and significance of Silurian--Early Devonian hinterland-directed deformation in the internal Humber zone of the southern Quebec Appalachians, *Can. Journ. of Earth Sci.,* 40, 2, 255.

Cook, F.A., White, D.J., Jones, A.G., Eaton, D.W.S., Hall, J., Clowes, R.M. (2010), How the crust meets the mantle: Lithoprobe perspective on the Mohorovičić discontinuity and crust-mantle transition, *Can. J. Earth Sci.,* 47, 315-351.

Crotwell, H. P., T. J. Owens, and J. Ritsema (1999), The TauP toolkit: Flexible seismic travel- time and ray-path utilities, *Seismol. Res. Lett.*, 70, 2, 154–160.

Eaton, D.W., Dineva, S., Mereu, R. (2006), Crustal thickness and Vp/Vs variations in the grenville orogen (Ontario, Canada) from analysis of teleseismic receiver functions, *Tectonophysics,* 420, 1, 223-238.

Gurrola, H., Minster, B.J. (1998), Thickness estimates of the upper-mantle transition zone from bootstrapped velocity spectrum stacks of receiver functions, *Geophys. J. Int.,* 133, 31–43.

Higgins, M.D., van Breemen, O. (1998), The age of the Sept Iles layered mafic intrusion, Canada, *Journ. of Geo.*, 1998, 106, 4, 421-431.

Hodych, J.P., Cox, R.A. (2007), Ediacaran U–Pb zircon dates for the Lac Matapédia and Mt. St.-Anselme basalts of the Quebec Appalachians: support for a long-lived mantle plume during the rifting phase of Iapetus opening, *Can. Journ. Earth Sci.*, 44, 4, 565-58.

Hughes, S., Luetgert, J. (1991), Crustal structure of the western New England Appalachians and the Adirondack Mountains, *J. Geophys. Res.*, 96, 16, 471–494.

Hynes, A., Rivers, T. (2010), Protracted continental collision – Evidence from the Grenville orogen, *Can. Journ. Earth Sci.,* 47 , 5, 591-620.

Kennett, B.L.N., Engdahl, E.R., Buland, R. (1995), Constraints on seismic velocities in the Earth from traveltimes, *Geophys. Journ. Intl.,* 122, 1, 108-124.

Kumarapeli, P.S. (1993), A plume-generated segment of the rifted margin of Laurentia, Southern Canadian Appalachians, seen through a completed Wilson Cycle, *Tectonophysics*, 219, 1-3, 47-55.

Li, A., Fischer, K.M., Van Der Lee, S., Wysession, M.E. (2002), Crust and upper mantle discontinuity structure beneath eastern North America, *J. of Geophys. Res.,* 107, B5.

Liggoria, J.P., Ammon, C.J. (1999), Iterative deconvolution and receiver-function

estimation, *Bull. Seism. Soc. Am.*, 89, 5, 1395-1400.

Mereu, R.F., Wang, D., Kuhn, 0., Forsyth, D. (1986), Summary of the results of the 1982 long range seismic experiment across the Ottawa-Bonnechere graben and western Grenville Front. In: J.M. Moore, A. Davidson and A.J. Baer (Editors), The Grenville Province, *Geol. Assoc. Can., Spec. Pap.,* 31, 235-240.

Musacchio, G., Mooney, W.D., Luetgert, J. H., Christensen, N. I. (1997), Composition of the crust in the Grenville and Appalachian provinces of North America inferred from Vp /Vs ratios, *J. Geophys. Res.*, 102, 15,225–15,241.

Owens, T.J., Zandt, G. (1985), The response of the continental Crust-Mantle boundary observed on broadband teleseismic receiver functions, *Geophys. Res. Lett.,* 12, 10, 705-708.

Pinet, N., Tremblay, A. (1995), Tectonic evolution of the Quebec-Maine Appalachians – From oceanic spreading to obduction and collision in the northern Appalachians, *Am. Journ. of Sci.*, 295, 2, 173-200.

Park, J., Levin, V. (1997), *P-SH* conversions in a flat-layered medium with anisotropy of arbitrary orientation, *Geophys. J. Int.,* 131, 253-266.

Park, J., Levin V. (2000), Receiver functions from multiple-taper spectral correlation estimates, *Bull. Seism. Soc. Am.*, 90, 1507–1520.

Petrescu, L., Bastow, I.D., Darbyshire, F.A., Gilligan, A., Bodin, T., Menke, W., Levin, V. (2015), Three billion years of crustal evolution in eastern Canada: Constraints from receiver functions, *J. Geophys. Res. Solid Earth,*121, doi:10.1002/2015JB012348.

Prave, A.R., Kessler, L.G., Malo, M., Bloechl, W.V. Riva, J. (2000), Ordovician arc collision and foredeep evolution in the Gaspe Peninsula, Quebec: the Taconic Orogeny in Canada and its bearing on the Grampian Orogeny in Scotland, *Journ. of the Geo. Soc.*, 157, 393-400.

Razi, A.S., Levin, V., Roecker, S.W., Huang, G.D. (2014), Crustal and uppermost mantle structure beneath western Tibet using seismic traveltime tomography, *Geochem., Geophys., Geosys.: G3*, 15, 2, 434-452.

Rondenay, S., Bostock, M., Hearn, G., White, D., Ellis, R. (2000), Lithospheric assembly and modification of the SE Canadian Shield: Abitibi–Grenville teleseismic experiment, *J. Geophys. Res.,* 105, 13735–13754.

Taylor, S.R., Toksoz, N.F. (1982), Crust and upper-mantle velocity structure in the Appalachian orogenic belt: Implications for tectonic evolution, *Geo. Soc. of Am.,* 93, 315-329.

Tesauro, M., Kaban, M.K., Mooney, W.D., Cloetingh, S. (2014), NACr14: A 3D model for the crustal structure of the North American Continent, *Tectonophysics*, 631, 65-86.

White, D.J., Forsyth, D., Asudeh, I., Carr, S.D., Wu, H., Easton, R.M., and Mereu, R.F. (2000),t A seismic-based cross-section of the Grenville Orogen in southern Ontario and western Quebec. *Can. Journ. of Earth Sci.,* **37**, 2–3, 183–192. doi:10. 1139/cjes-37-2-3-183.

Whitehead, J., Spray, J.G., Reynolds, P.H. (1996), 40Ar/39Ar age constraints on Taconian and Acadian events in the Quebec Appalachians, *Geology*, 24, 4, 359-362

Whitmeyer, S.J., Karlstrom, K.E. (2007), Tectonic model for the Proterozoic growth of North America, *Geosphere*, 3, 4, 220-259.

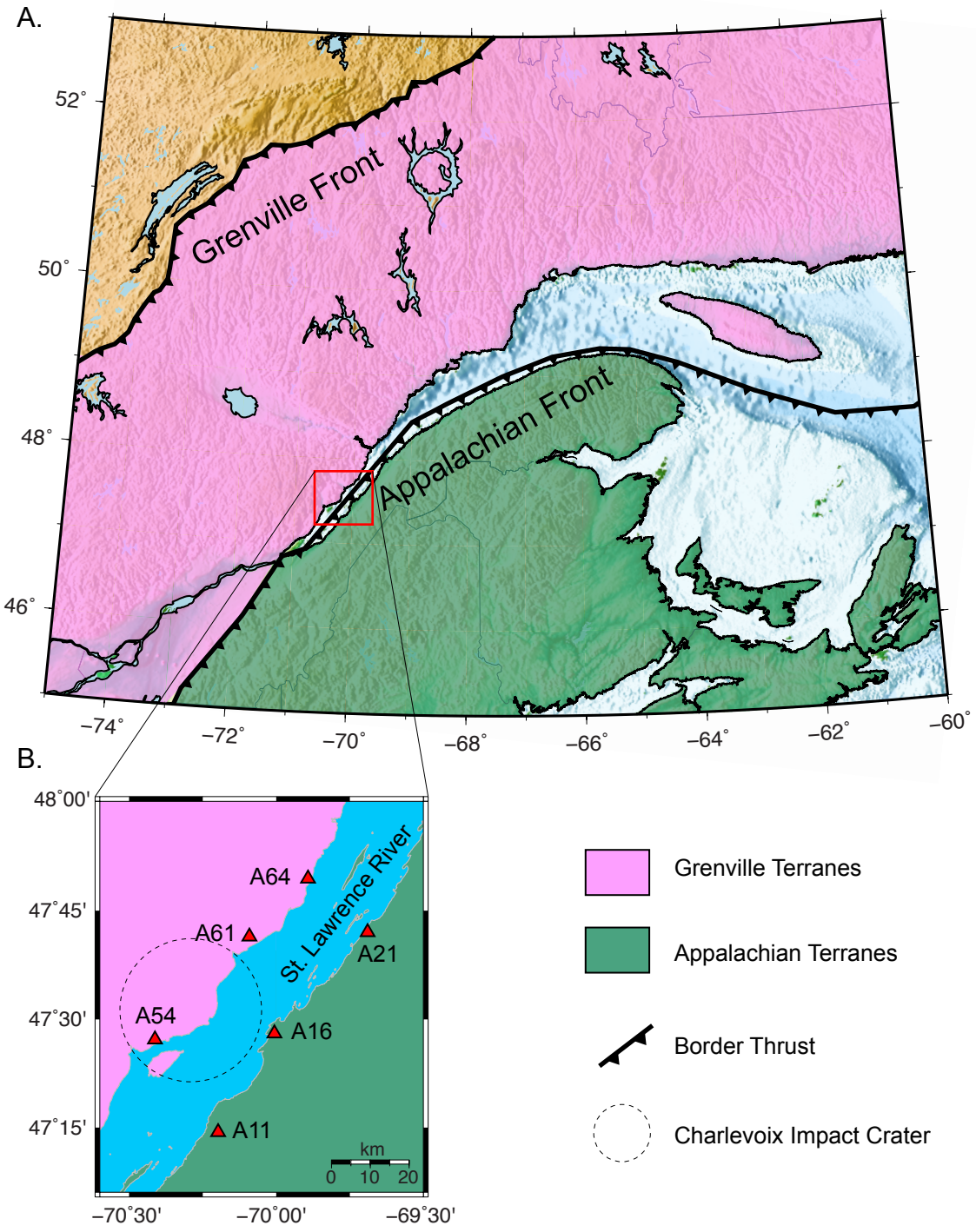


Figure 1: Regional and local map of the study area. A) Tectonic map of north eastern North America. B) A local map of the study area. Red triangles represent the locations of the seismic observatories used in this study.

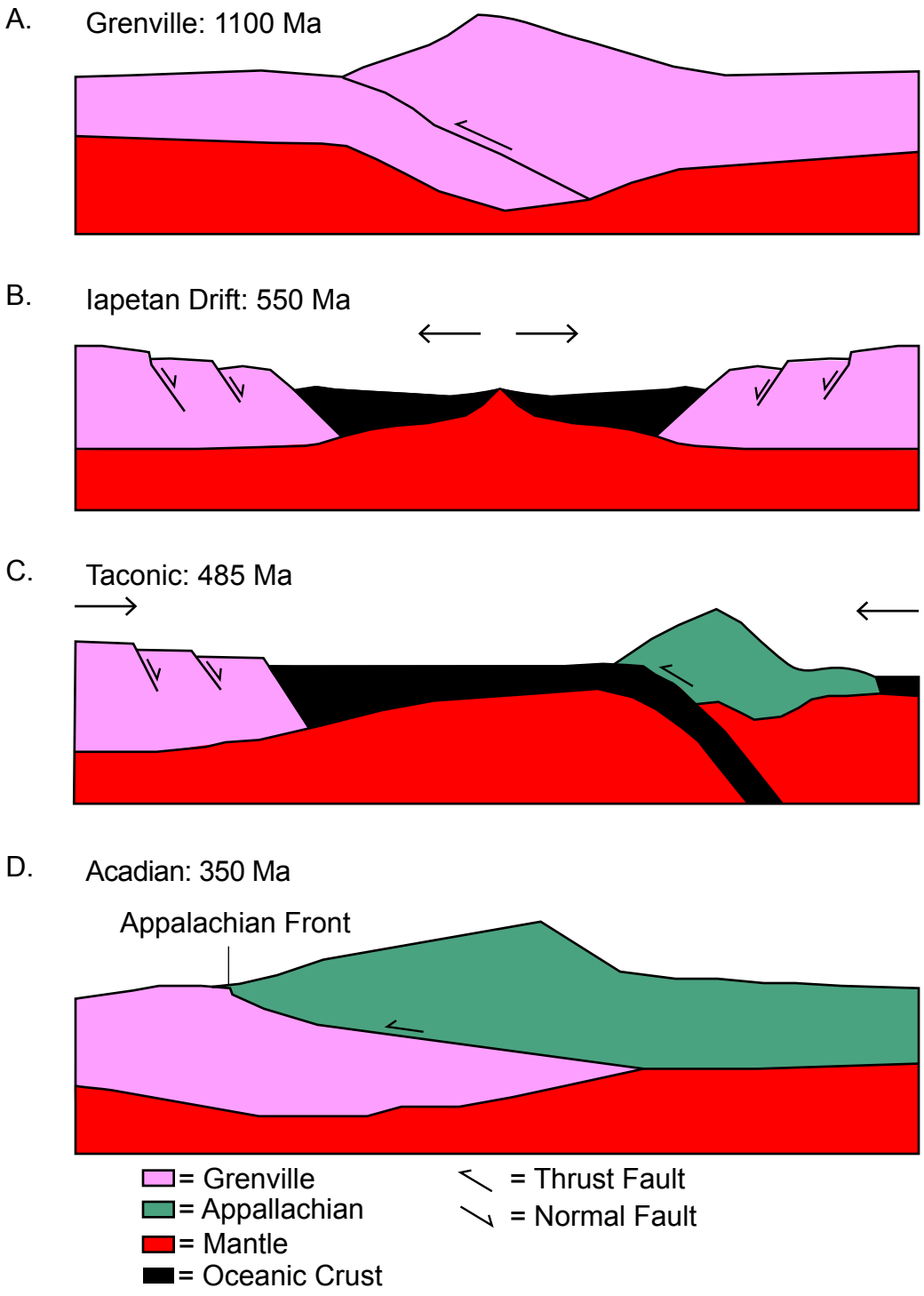


Figure 2: Four phase tectonic history of the St. Lawrence river. A) Setting at the end of Grenville (Hynes & Rivers, 2010). B) Setting during Iapetus ocean formation (Kumarapeli, 1989). C) Taconic arc formation (Whitehead et. al., 1996). D) End of acadian orogen (Whitehead et. al., 1996)

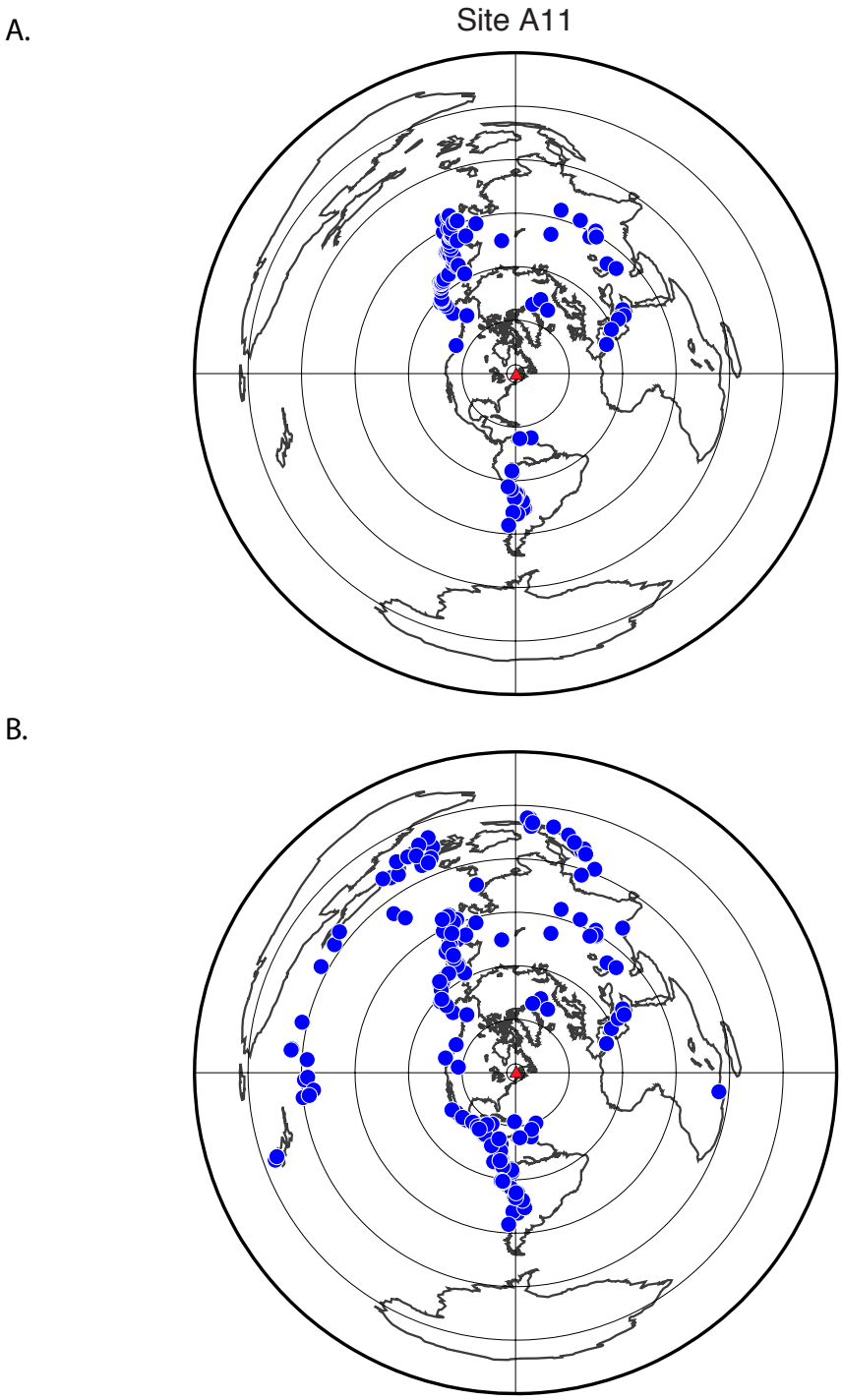


Figure 3: A) Map of sources (blue circles) used to compute epicentral RFs centered on site A11 (red triangle). Back- azimuth ranges used are 300 °- 350 °, 020°-080°, and 170°-190°. Epicentral distances range from 40°-100° . B) Map of sources used to compute a back-azimuthal gather at site A11. Back-azimuths range from 0°-360°.

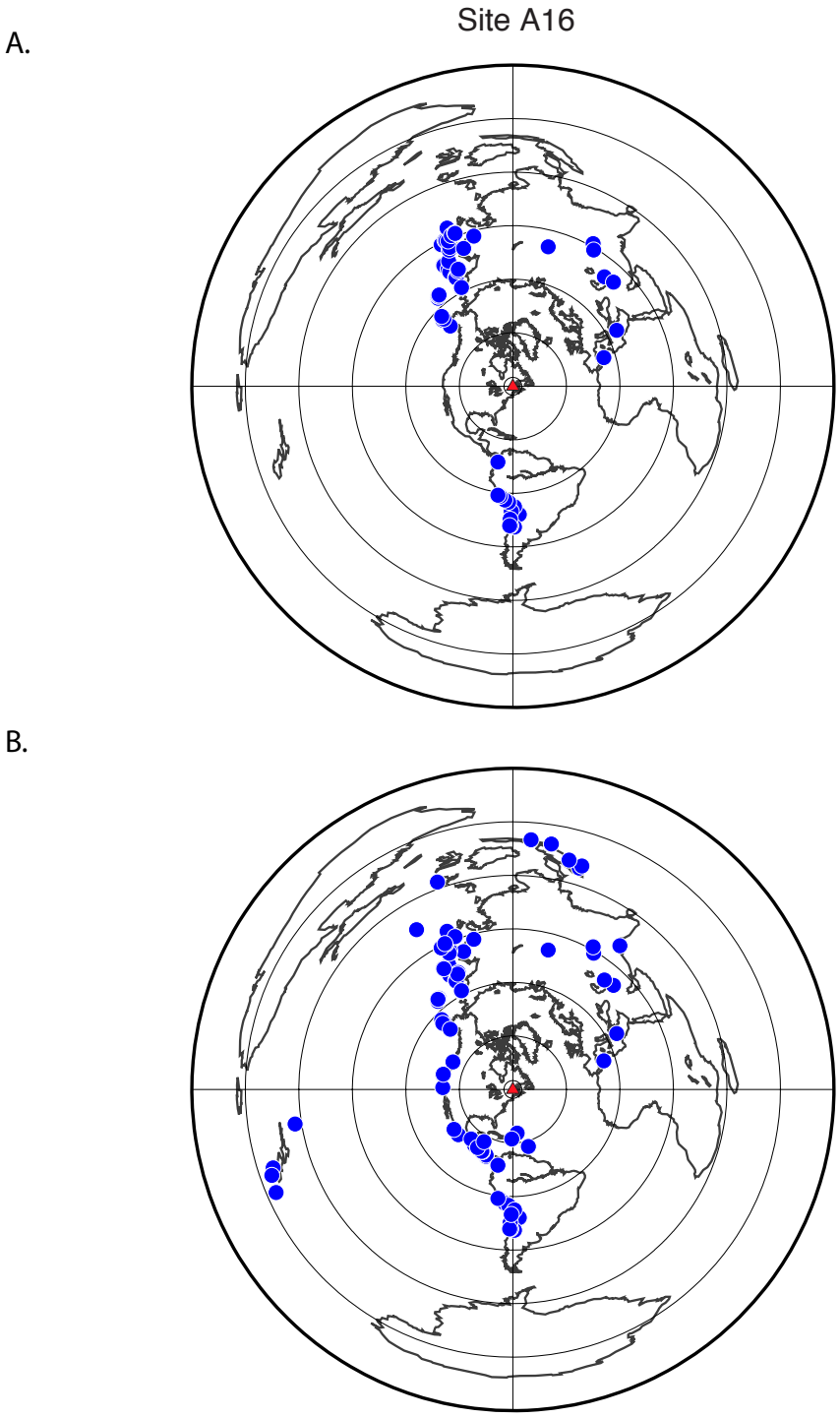


Figure 4: A) Map of sources (blue circles) used to compute epicentral RFs centered on site A16 (red triangle). Back- azimuth ranges used are 300°-350°, 015°-075°, 164°-195.° Epicentral distances range from 40°-100° . B) Map of sources used to com- pute a back-azimuthal gather at site A16. Back-azimuaths range from 0°-360°.

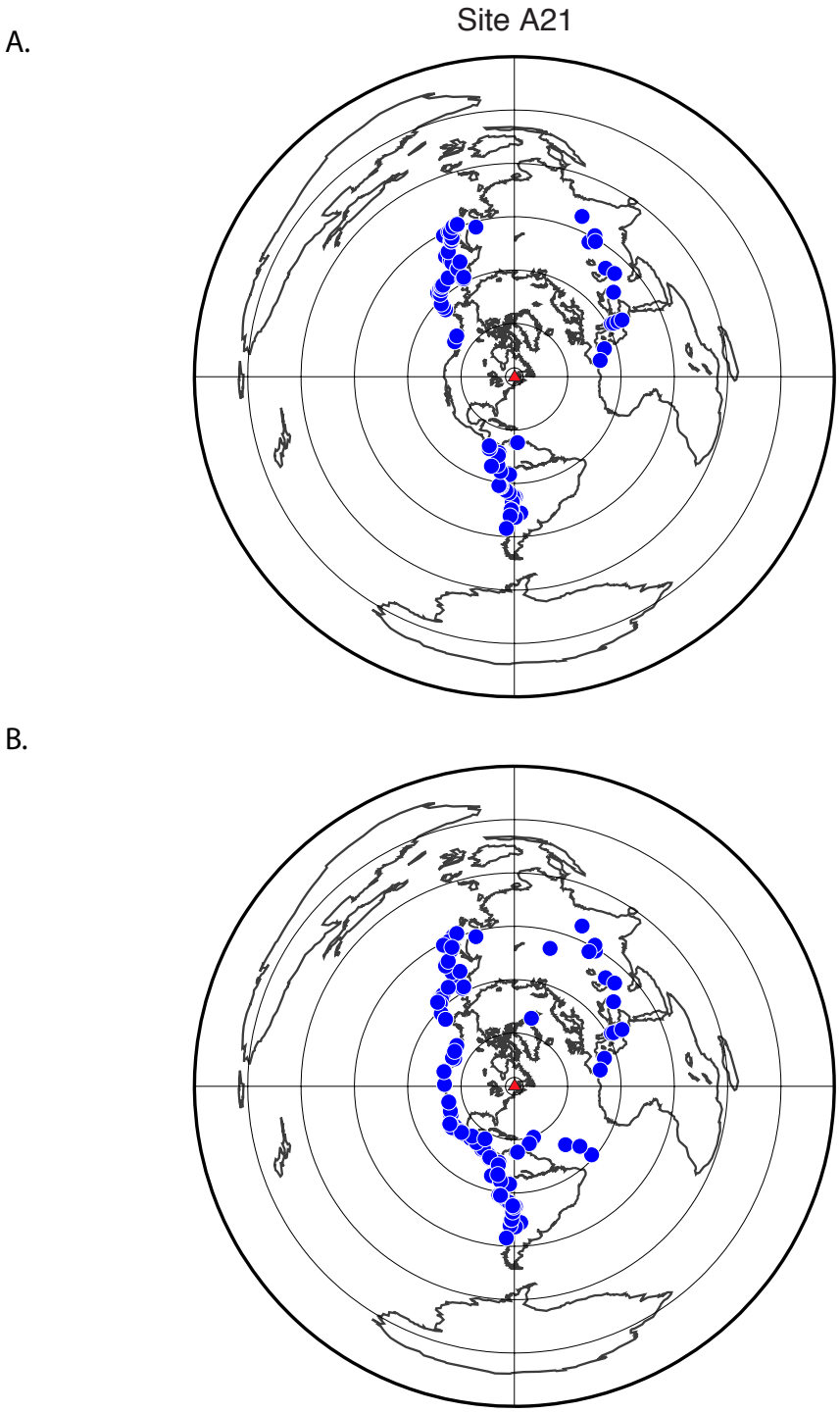


Figure 5: A) Map of sources (blue circles) used to compute epicentral RFs centered on site A21 (red triangle). Back- azimuth ranges used to compute RFs are 300°-350°, 020°-080°, and 170°-200° degrees. Epicentral distances range from 40°-100°. B) Map of the sources used to computed a back-azimuthal gather at site A21. Back-azimuths range from 0°-360°.

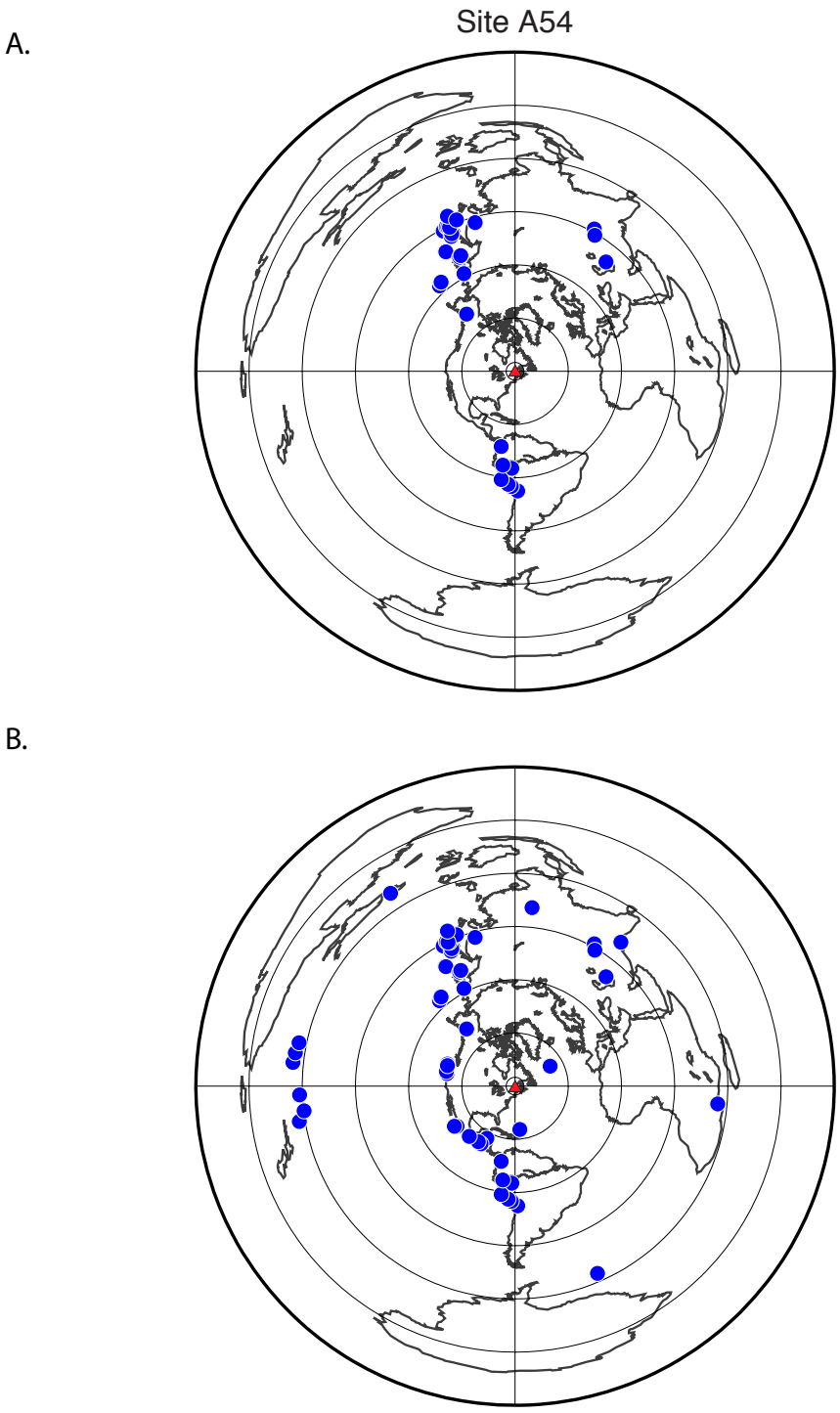


Figure 6: A) Map of sources (blue circles) used to compute epicentral RFs centered on site A54 (red triangle). Back- azimuth ranges used are 300°-350°, 030°-050°, and 170°-190° . Epicentral distances range from 40°-100° degrees. B) Map of sources used to compute a back-azimuthal gather at site A54. Back-azimuths range from 0°-360°.

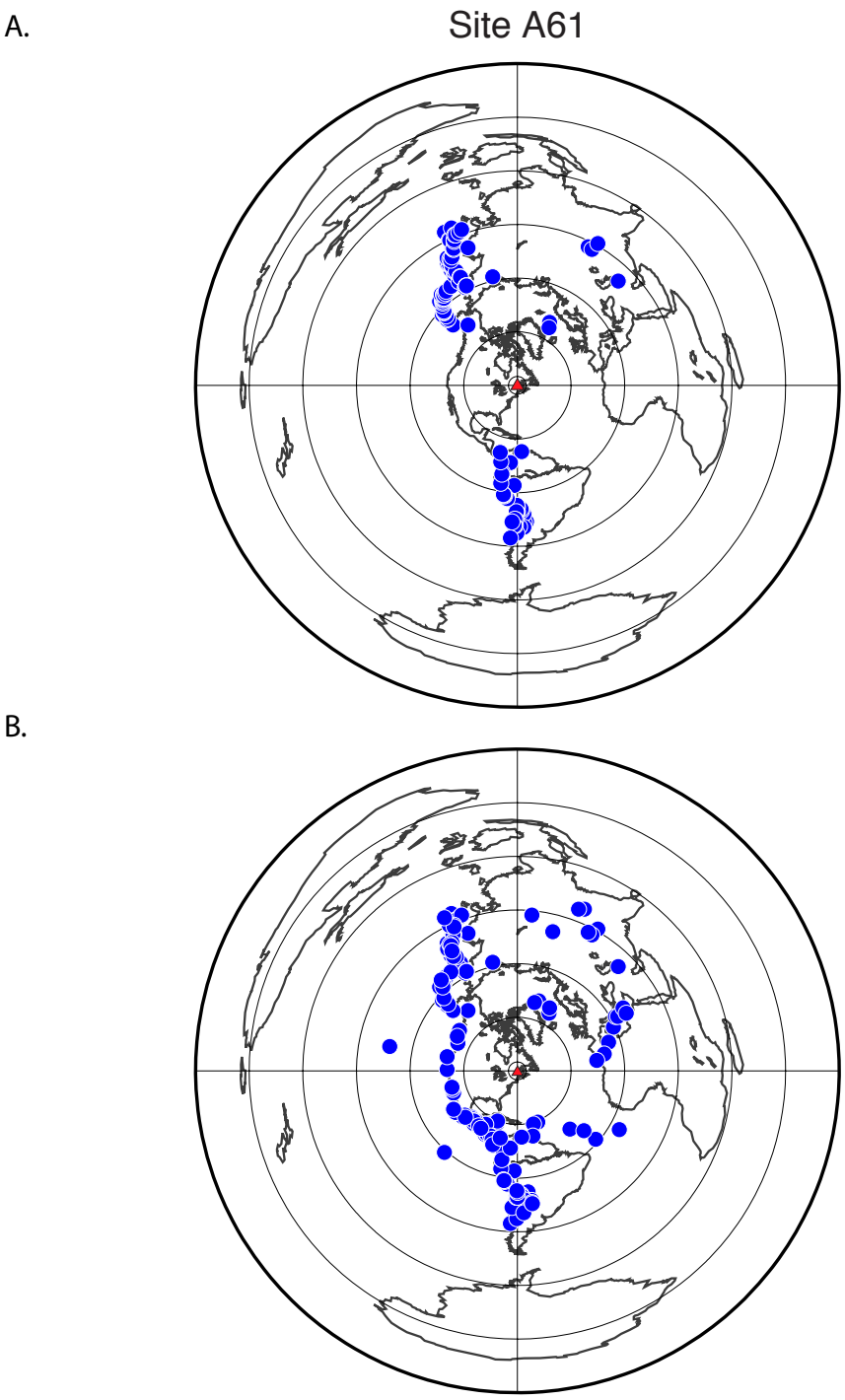


Figure 7: A) Map of sources (blue circles) used to compute epicentral RFs centered on site A61 (red triangle). Back azimuth ranges used are 310°-340°, 020°-080°, and 170°-190°. Epicentral distances range from 40°-100° . B) Map of sources used to com- pute a back-azimuthal gather at site A61. Back-azimuths range from 0°-360°.

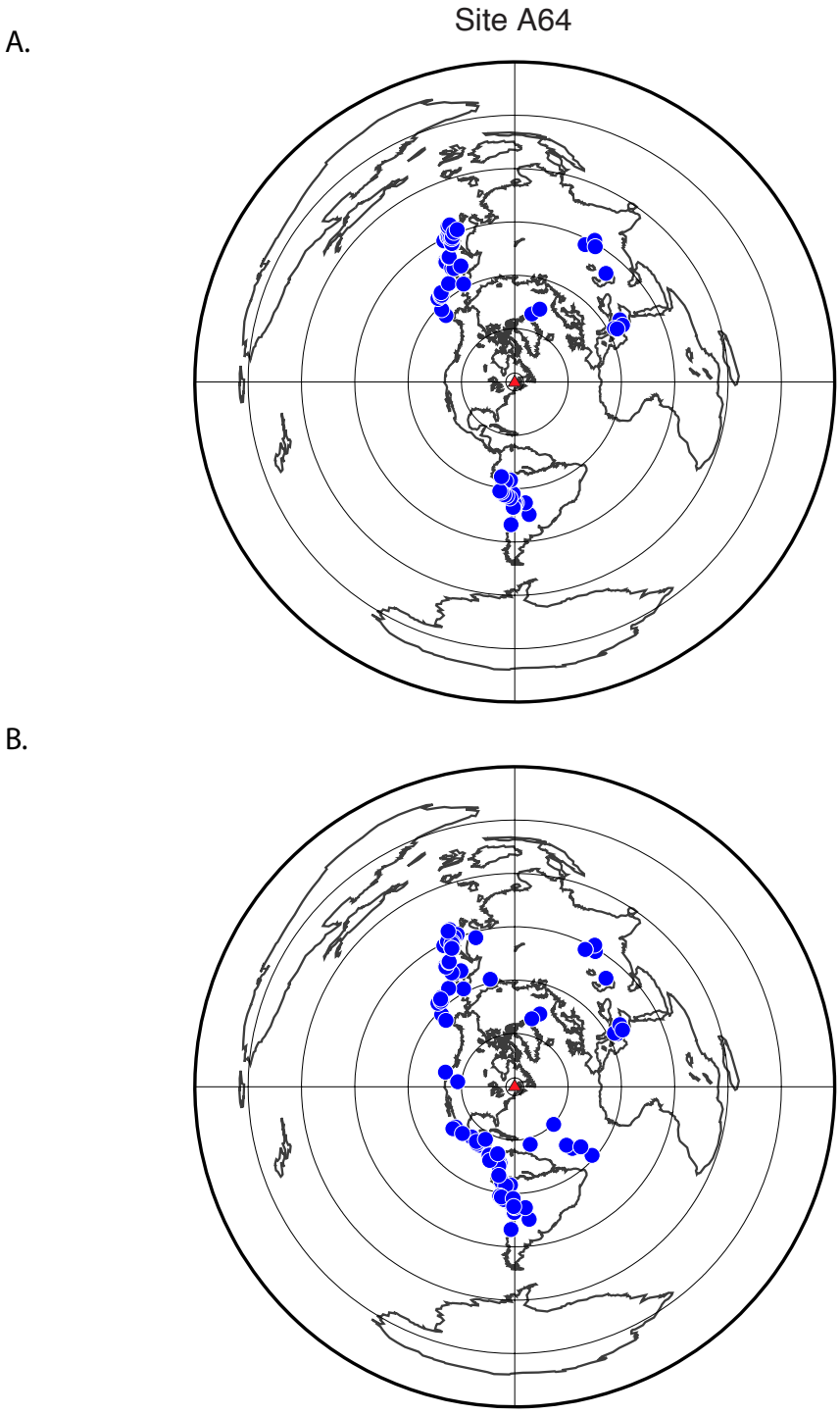


Figure 8: A) Map of sources (blue circles) used to compute epicentral RFs centered on site A64 (red triangle). Back azimuth ranges used are 310 °- 340 °, 010°-065°, and 170°-190°. Epicentral distances range from 40°-100°. 9B. B) Map of sources used to compute a back-azimuthal gather at site A64. Back-azimuths range from 0°-360°.

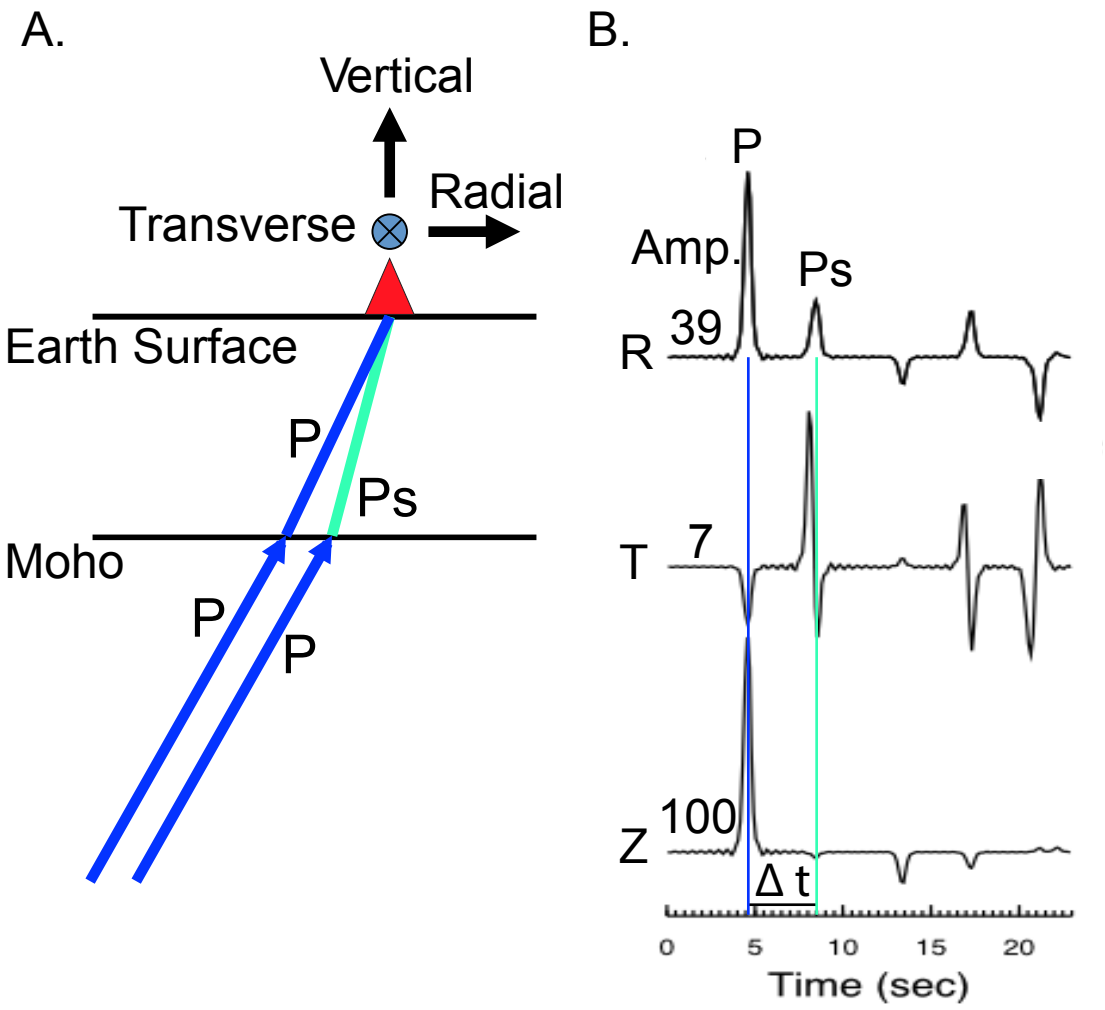


Figure 9: Schematic diagram of receiver function geometry and seismograms (Modified from Park and Levin, 1997). A) Simplified cross-section of RF geometry along the radial receiver component. Shows P (blue) to Ps (green) wave conversion and refraction during transmission through the Moho discontinuity and arrival at the receiver (red triangle). The time delay between the P and Ps wave is a result of the difference in seismic velocities of the two phases. The P-wave travels a longer path, through the crust at higher seismic velocity than the Ps wave. B) Seismograms of the Radial, Vertical and Transverse components. The P and Ps waves are highlighted with the blue and green lines, respectively. The time delay between the P and Ps wave records on the radial and vertical components is indicative of depth to the boundary that produced the conversion.

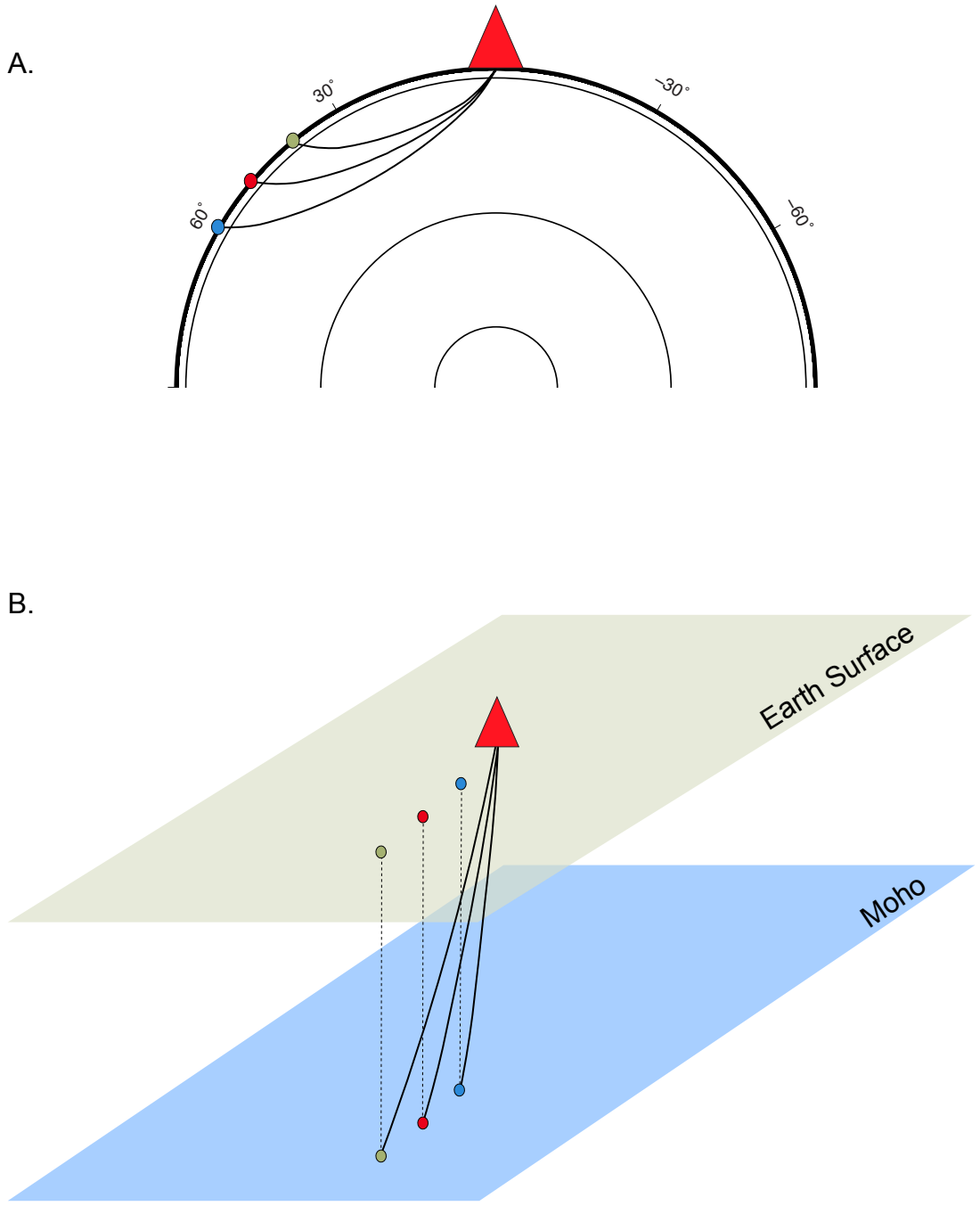


Figure 10: Ray path geometry of modeled P-waves A) Direct P-wave ray paths from sources (colored circles) to receiver (red triangle), with epicentral distances of 40, 50, and 60 degrees. The outer most circle is representative of the Moho discontinuity in B. B). Simplified schematic diagram showing Ps rays corresponding to epicentral RFs used to map a planar Moho as they approach the receiver (red triangle). The steepest ray approaches from a distance of 60 degrees. Events originating closer to the receiver generate shallower incidence angles than more distant sources. Colored dots correspond to the locations of each ray as they pierce the Moho.

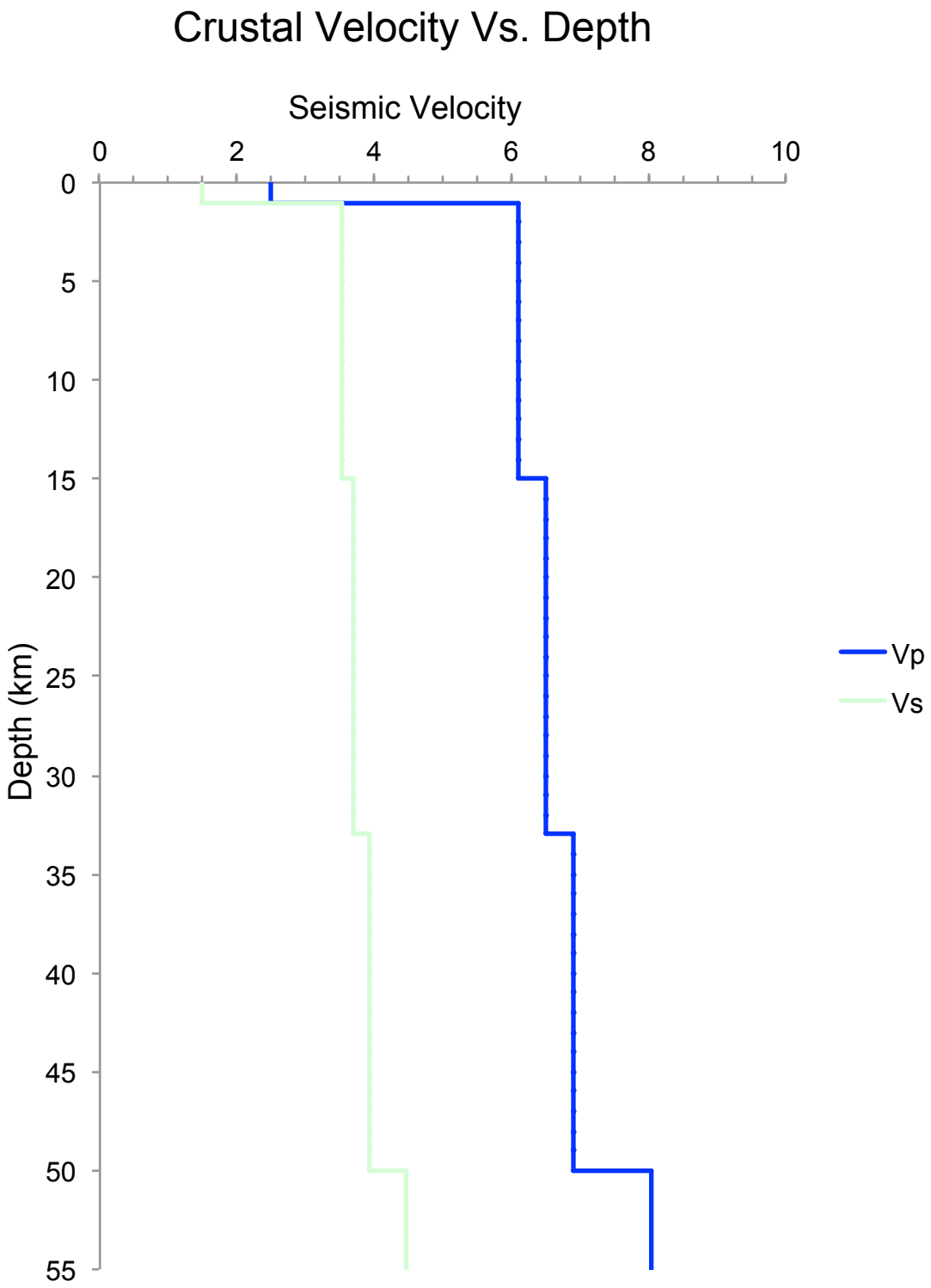


Figure 11: Crustal velocity vs. depth graph. Modeled 1D crustal velocity structure used for delay time to depth conversion (modified from Tesauro et. al., 2014). The crust is divided into upper, middle and lower-crust sub layers. Proportional thickness and Vp and Vs values of each sub-layer are maintained from Tesauro et. al., (2014). The absolute thickness of each sub-layer is modified to extend the total crustal thickness from 35 km to 50 km.

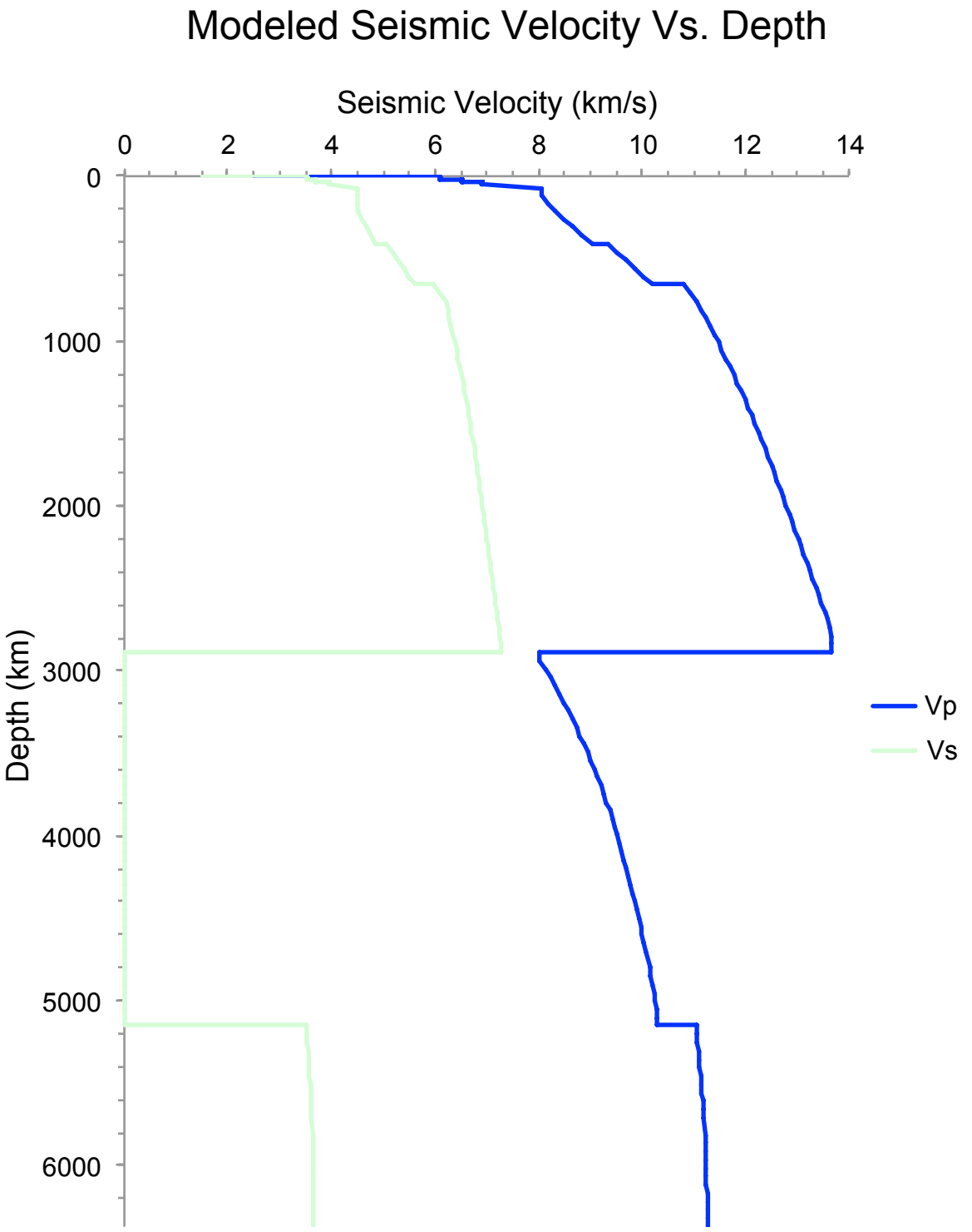


Figure 12: Velocity vs depth graph of the modified ak135 whole-Earth velocity model (modified from Kennett et. al., 1995). This model is used in this study to compute travel times in TauP (Crotwell et. al., 1999). The velocity structure below the Moho is consistent with the original ak135 model. See Fig. 11 for detailed modeled crustal velocity structure.

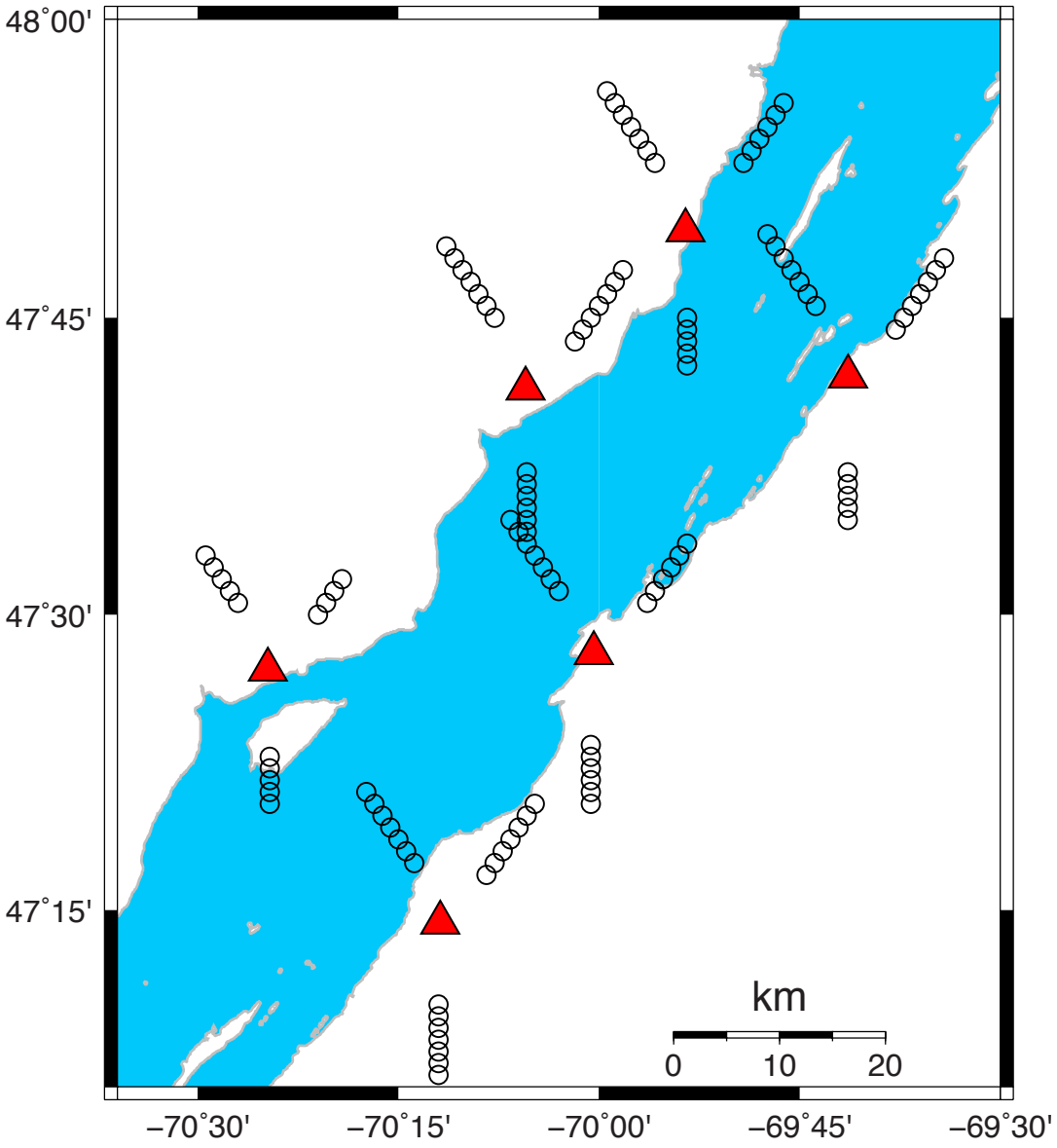


Figure 13: Map of receiver (red triangles) and Ps conversion (empty circles) locations at the base of the crust (50 km depth). Ps pierce points correspond to the interpreted Ps phases in the epicentral RFs (Figs. 15-20) . Pierce point locations are computed for rays from events with back-azimuths of 40, 180, and 330 degrees and epicentral distances of 40, 50, 60, 70, 80, 90, and 100 degrees for ease of plotting. Up to three 15 km long epicentral projections are used per receiver, resulting in a data coverage area of 4400 $km^2$.

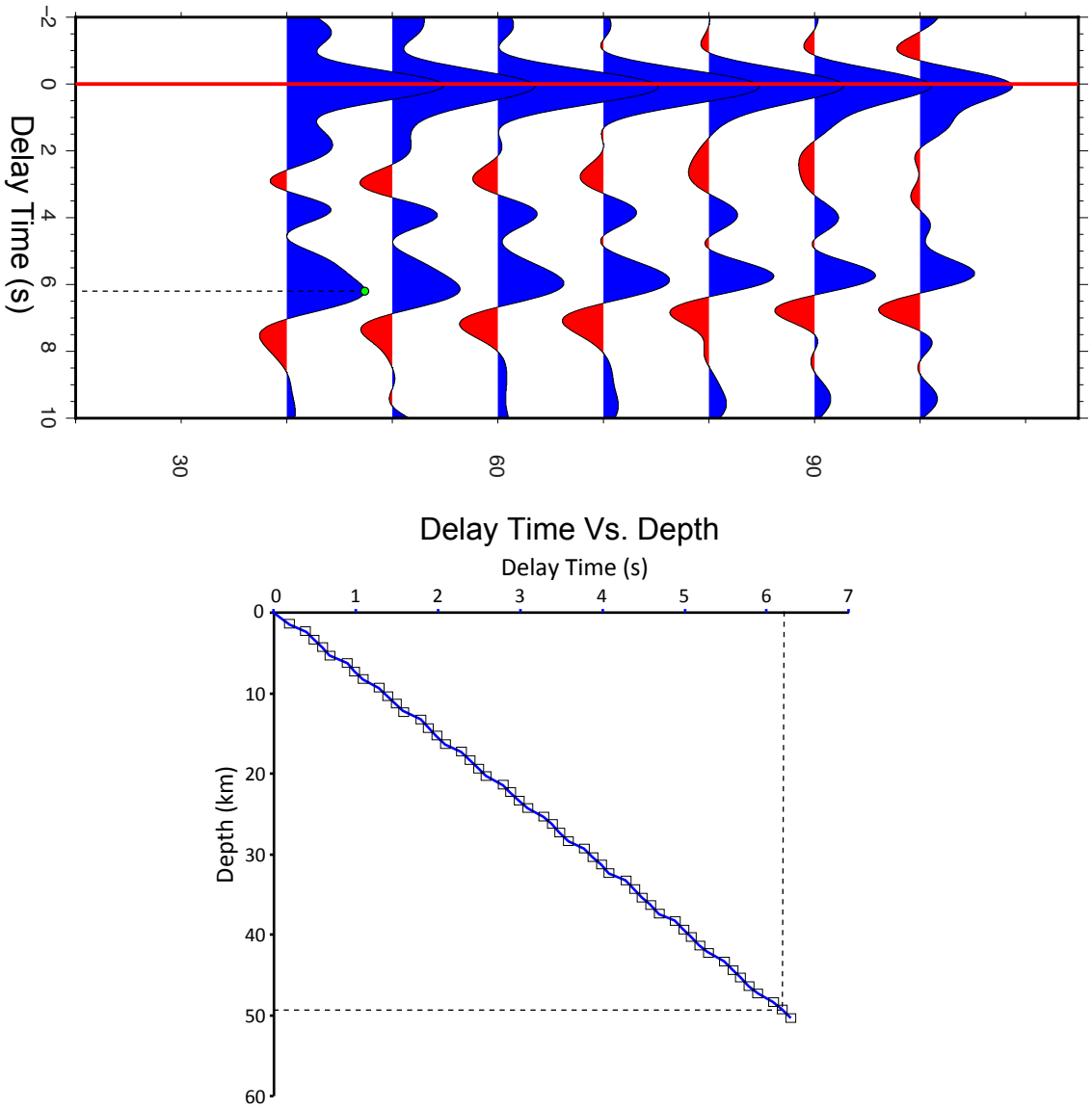


Figure 14: Time to depth conversion procedure. A) Interpreted RF delay time for a single bin (40° epicentral distance) . B) Modeled RF time vs. depth graph. Squares represent modeled delay times and their corresponding depths. The blue line is an interpolation between the discrete modeled data points.The dashed line is projected from the x-axis at the interpreted delay time from the RF to the closest modeled delay time. The dashed line projected to the y-axis represents the modeled depth corresponding to the interpreted delay time.

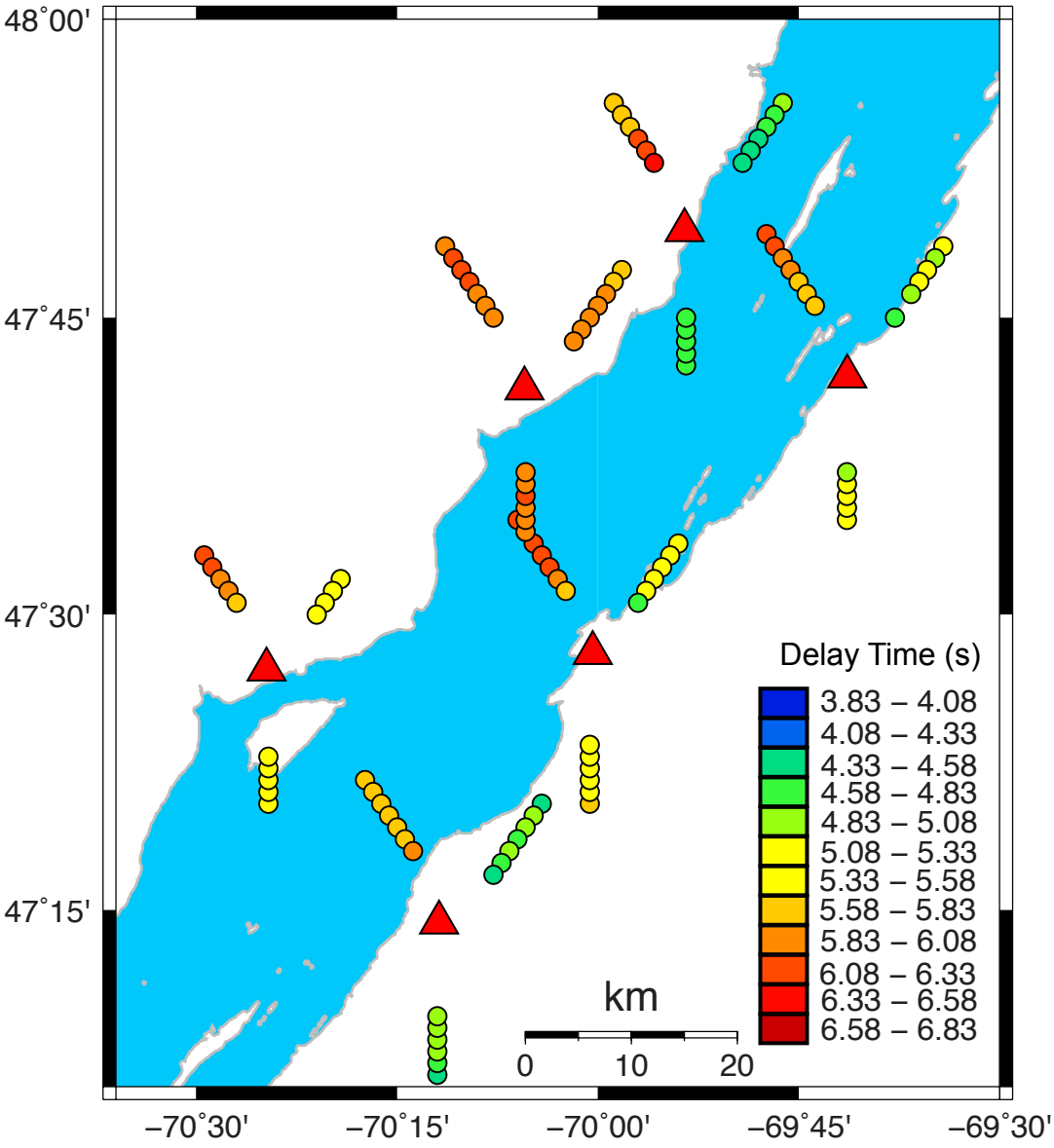


Figure 15: Map of recievers (red triangles) and Ps conversion points (circles) colored based on interpreted RF delay times from 1 Hz receiver functions.

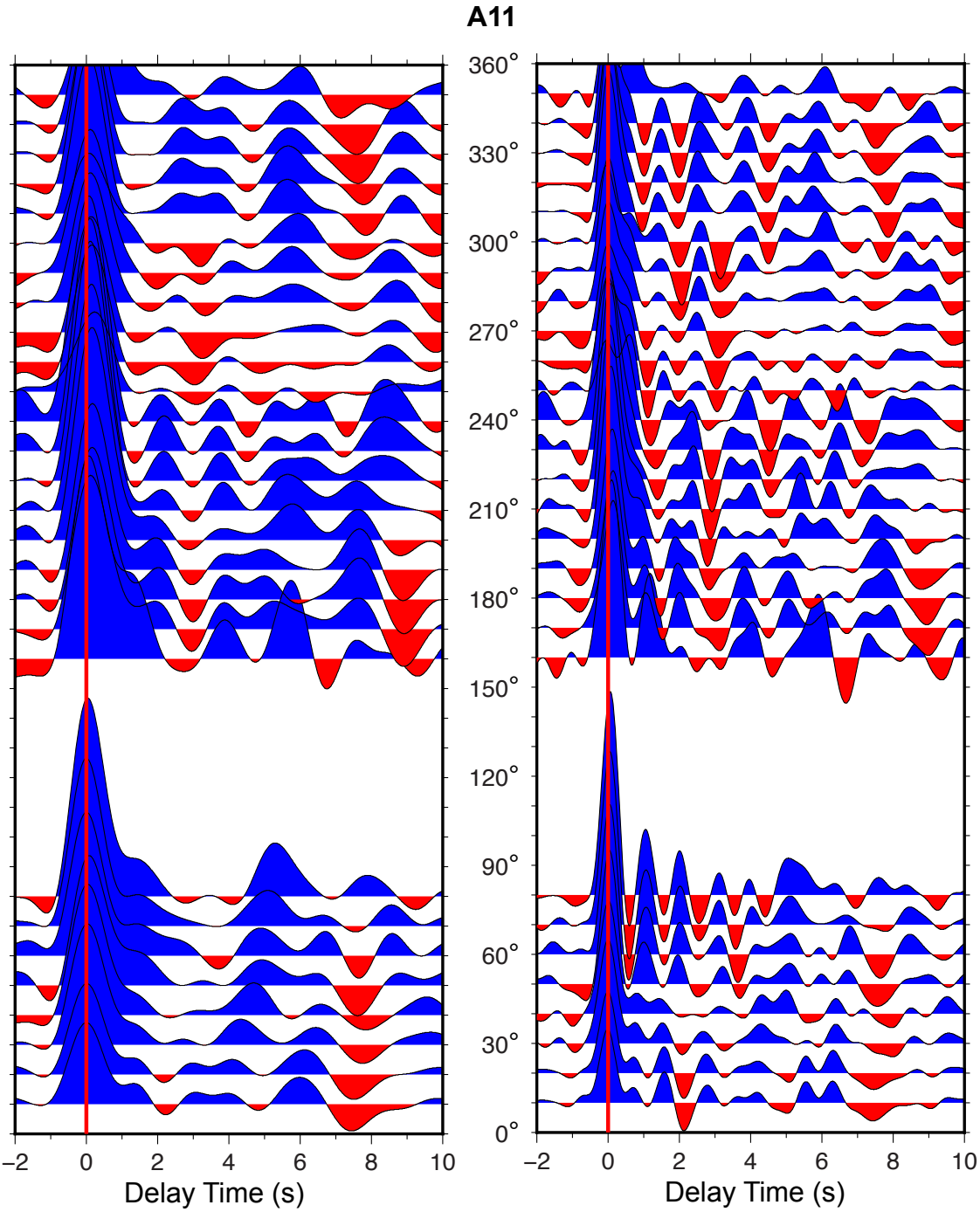


Figure 16: Back-azimuth reciever function gathers at site A11. The x-axis is delay time in seconds and the y-axis is event back-azimuth direction from 0°-360°.Reciever functions are filtered below 1 Hz (left) and 2 Hz (right). The red line set at 0 s indicates initial P-wave motion. No data were present between for back-azimuths between 090°-150°.

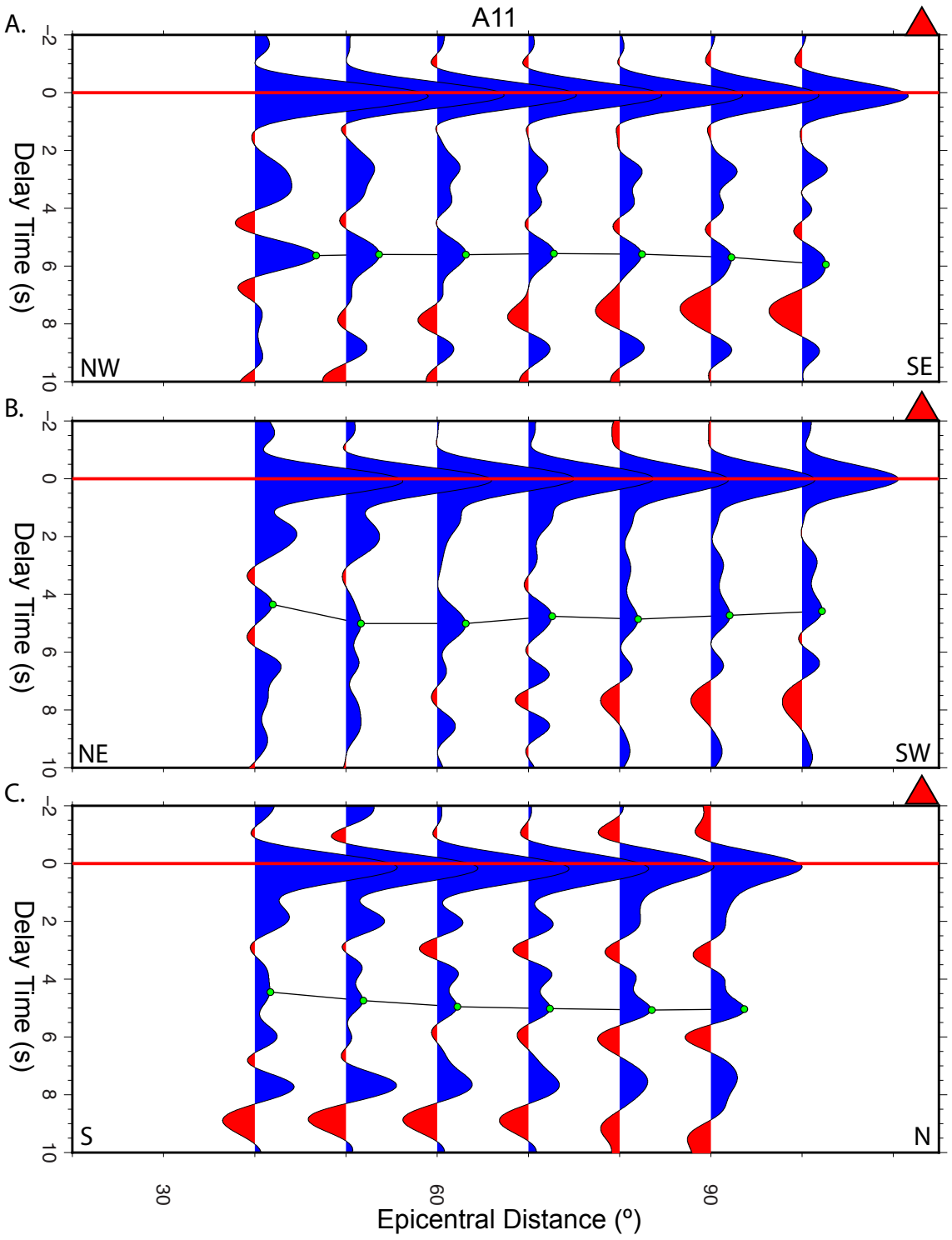


Figure 17: Interpreted epicentral receiver functions at site A11 filtered below 1 Hz. Red triangles represent the receiver locations relative to the profile. Red line at 0 s indicates the first recorded P-wave motion. Green circles indicate the positive phase interpreted as the Moho derived Ps phase. A) Back-azimuth ranges between 300°-350°. B) Back-azimuth ranges between 020°-080°. C) Back-azimuth ranges between 170°-190°.

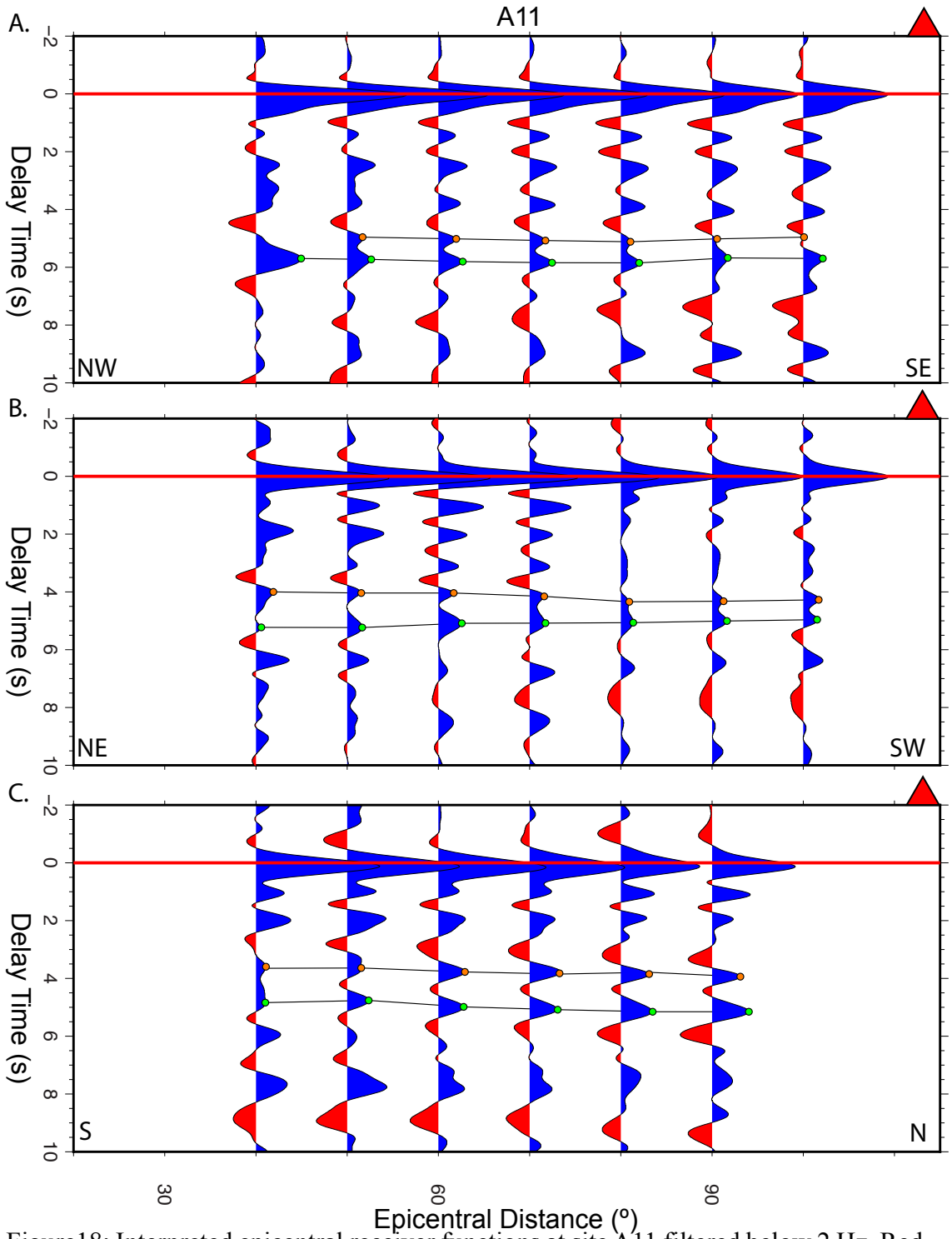


Figure18: Interpreted epicentral receiver functions at site A11 filtered below 2 Hz. Red triangles represent the receiver locations relative to the profile. Red line at 0 s indicates the first recorded P-wave motion. Green and orange circles indicate relative time delay of the positive Ps phases likely derived at the crust-manltle interface. A) Back-azimuth ranges between 300°-350°. B) Back-azimuth ranges between 20°-80°. C) Back-azimuth ranges between 170°-190°.

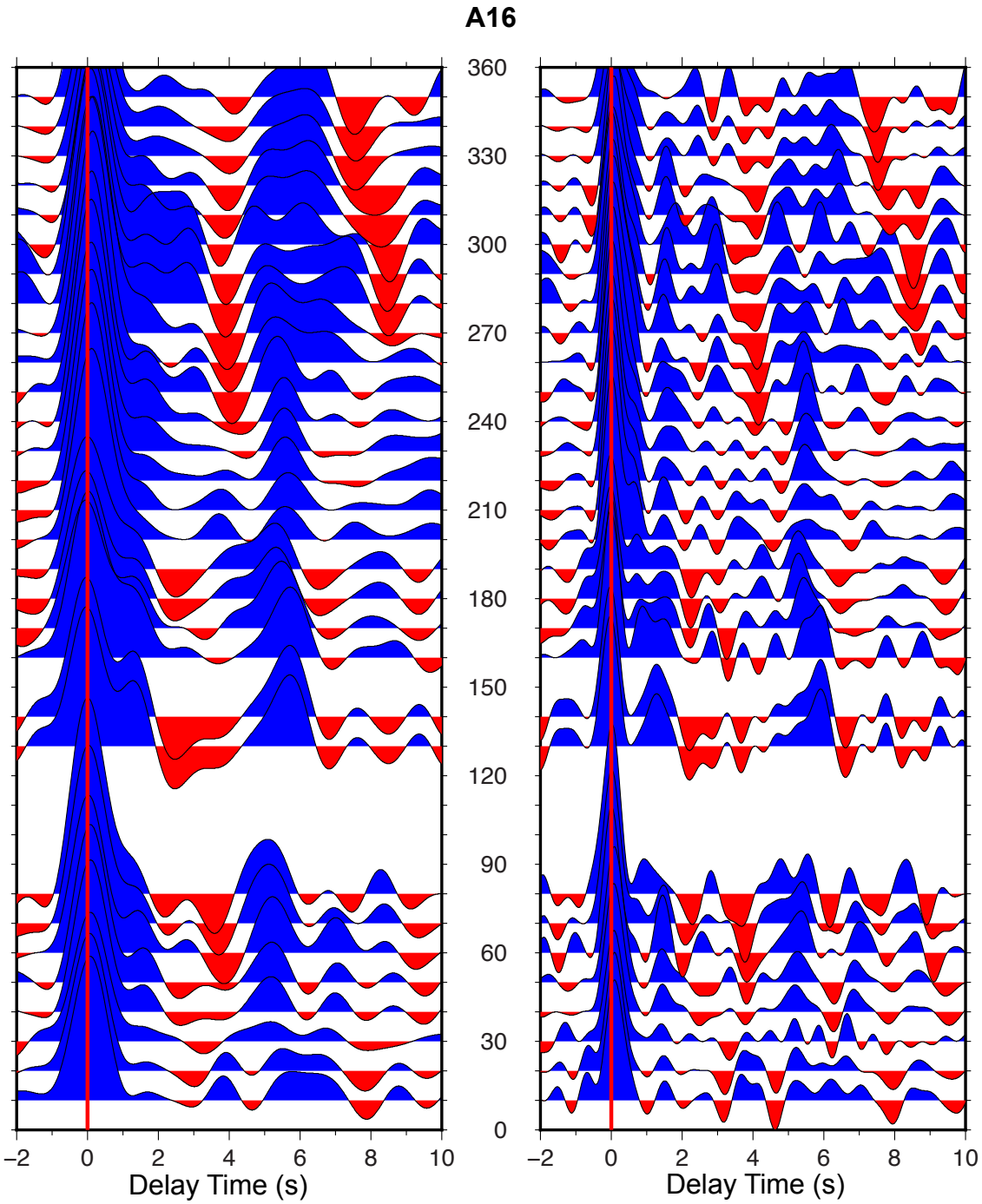


Figure 19: Back-azimuth reciever function gathers at site A16. The x-axis is delay time in seconds and the y-axis is event back-azimuth direction from 0°-360°.Reciever functions are filtered below 1 Hz (left) and 2 Hz (right). The red line set at 0 s indicates initial P-wave motion. No data were present between for back-azimuths of 150° and 90°-120°.

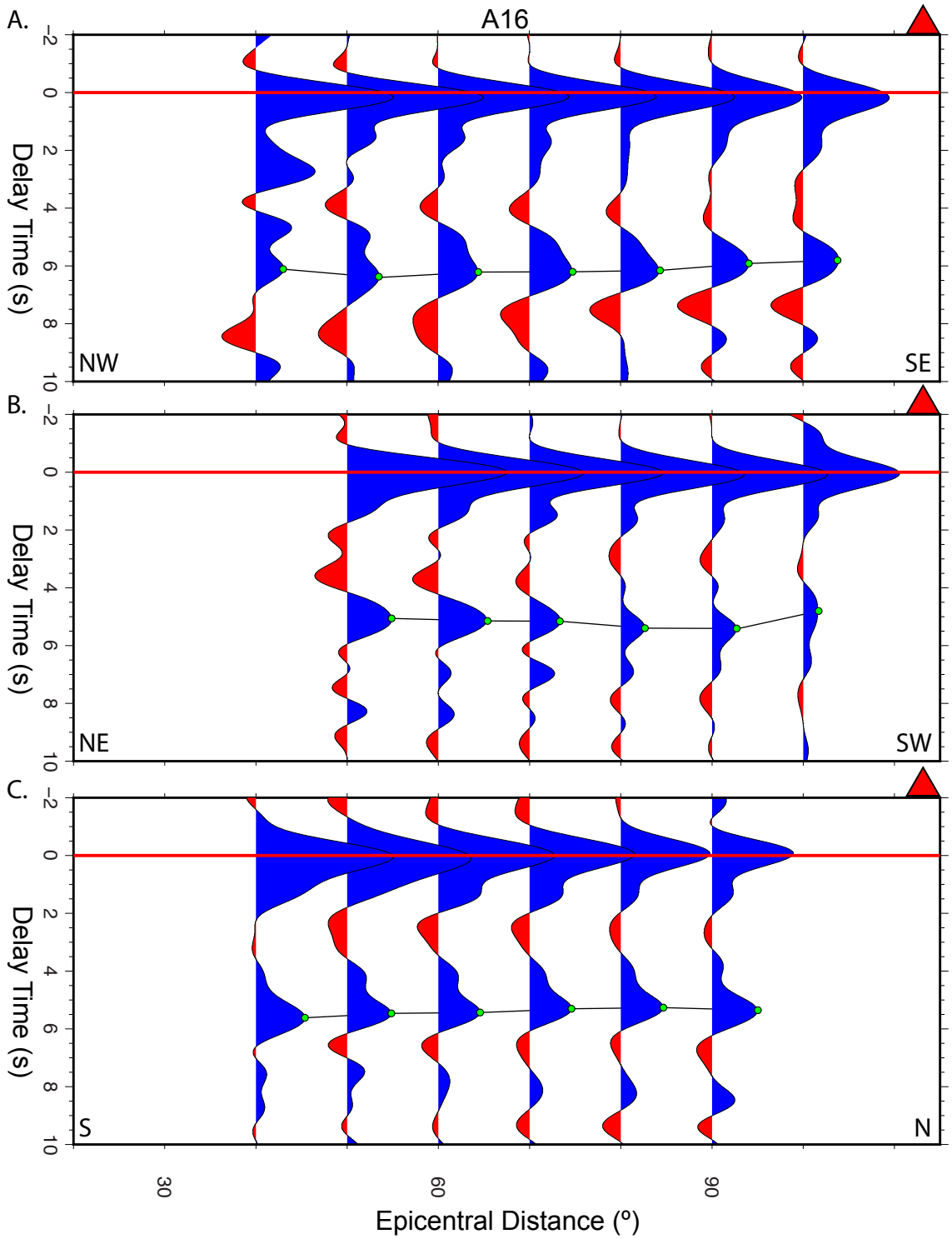


Figure 20: Interpreted epicentral receiver functions at site A16 filtered below 1 Hz. Red triangles represent the receiver locations relative to the profile. Red line at 0 s indicates the first recorded P-wave motion. Green dots indicate relative time delay of the positive phase interpreted as the Moho derived Ps phase. A) Back-azimuth ranges between 300°-350°. B) Back-azimuth ranges between 015°-075°. C) Back-azimuth ranges between 164°-195°.

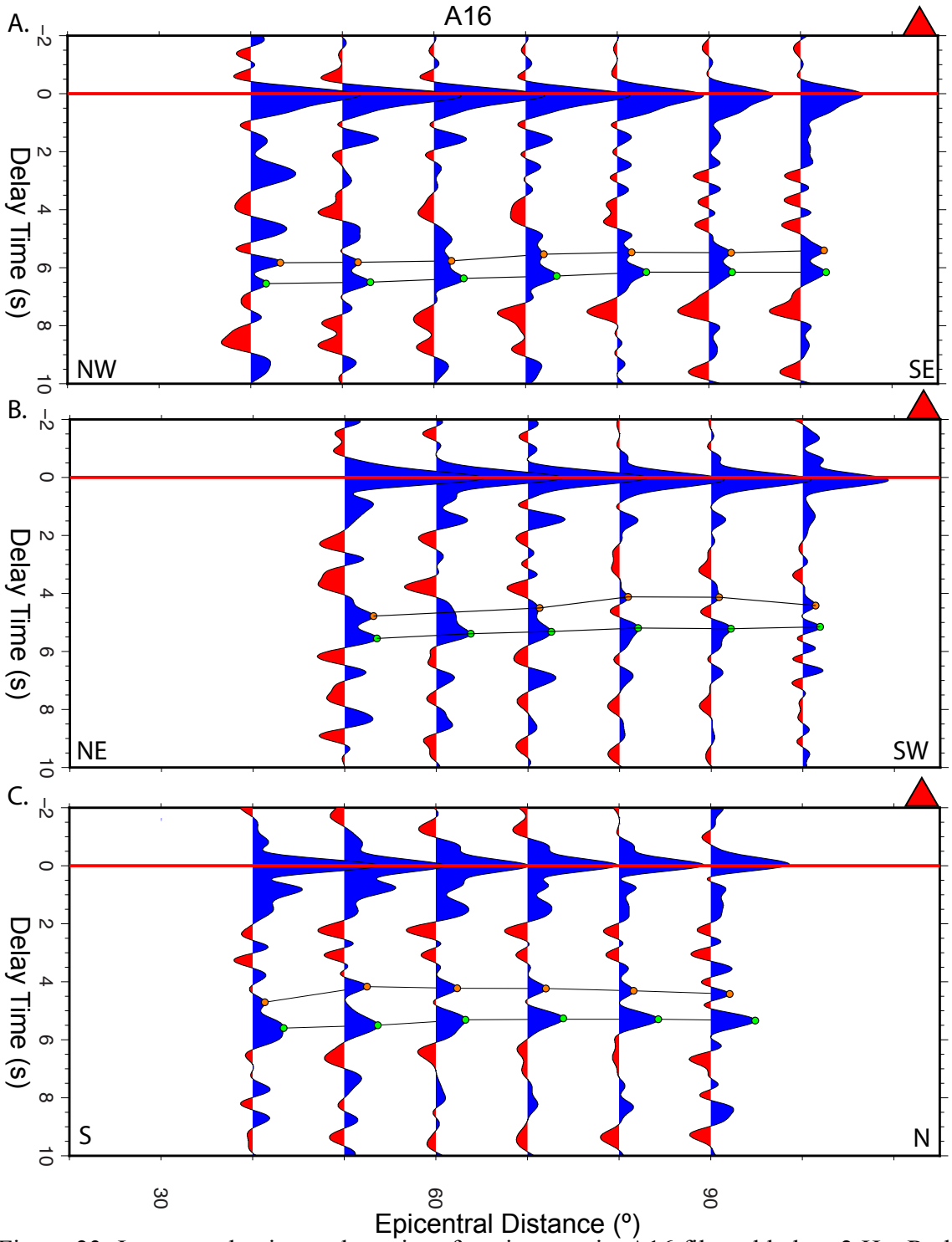


Figure 23: Interpreted epicentral receiver functions at site A16 filtered below 2 Hz. Red triangles represent the receiver locations relative to the profile. Red line at 0 s indicates the first recorded P-wave motion. Green and orange circles indicate relative time delay of the positive Ps phases likely derived at the crust-manltle interface. A) Back-azimuth ranges between 300°-350°. B) Back-azimuth ranges between 015°-075°. C) Back-azimuth ranges between 164°-195°.

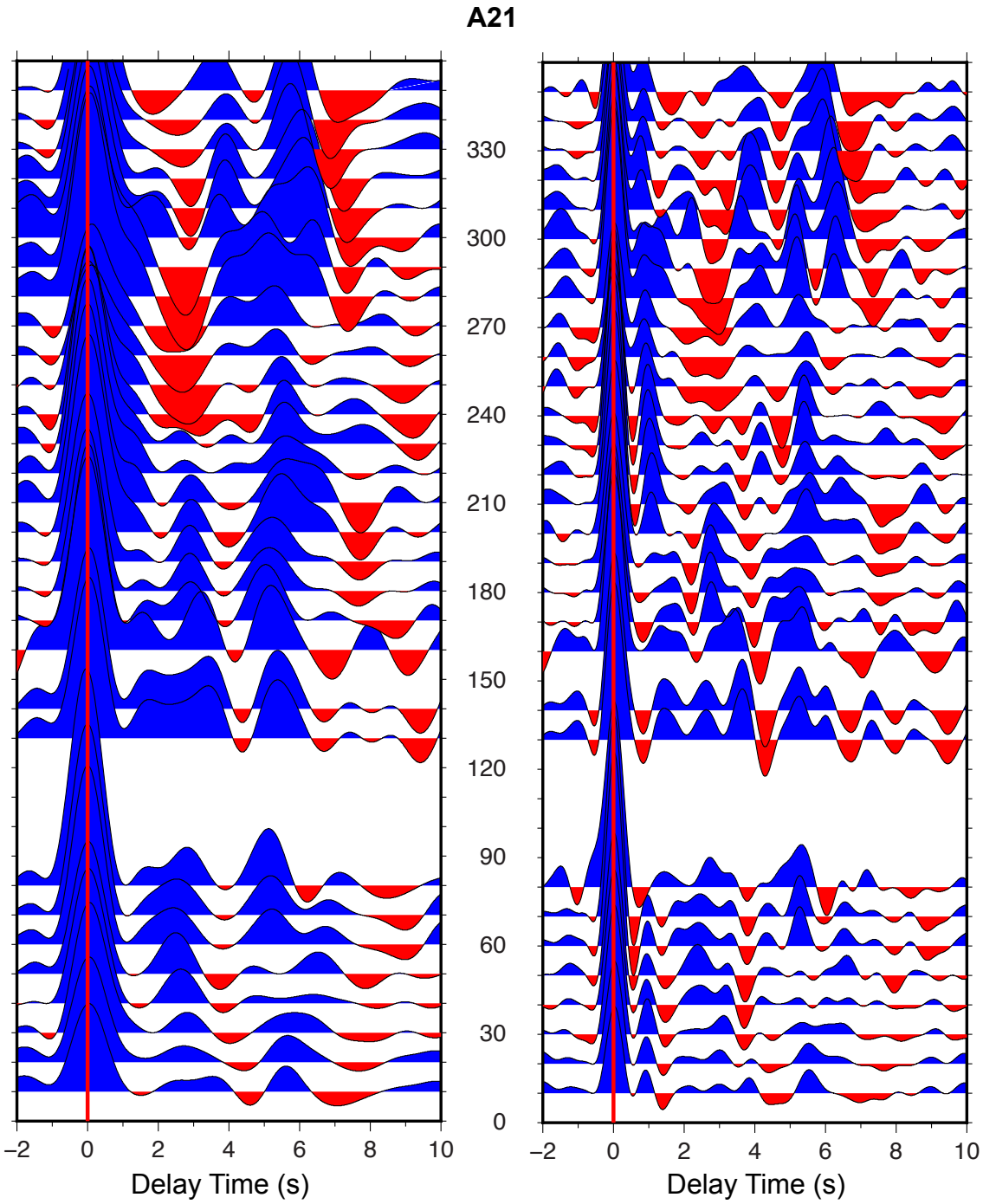


Figure 22: Back-azimuth reciever function gathers at site A21. The x-axis is delay time in seconds and the y-axis is event back-azimuth direction from 0°-360°. Reciever functions are filtered below 1 Hz (left) and 2 Hz (right). The red line set at 0 s indicates initial P-wave motion. No data were present between for back-azimuths of 150° and 90°-120°.

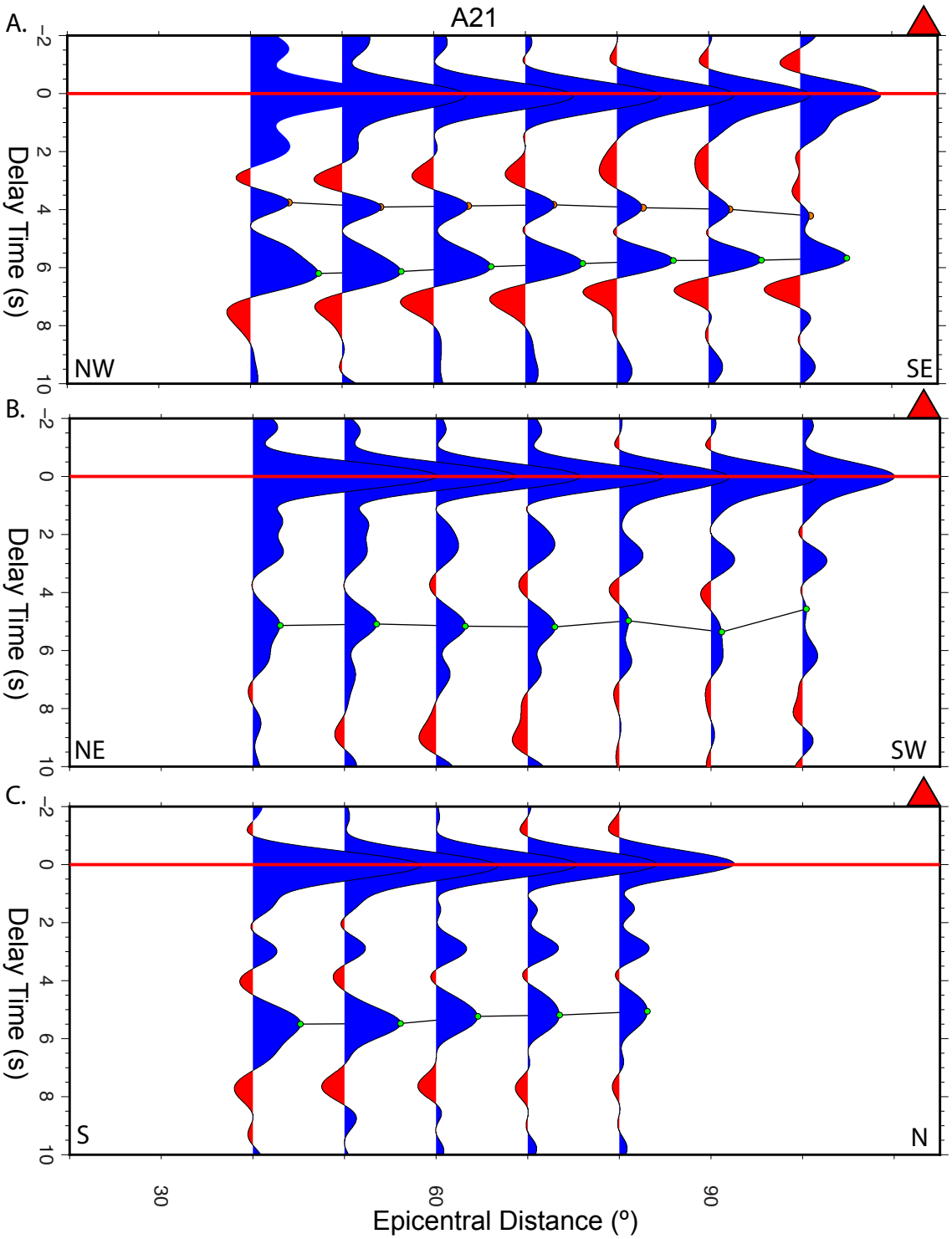


Figure 23: Interpreted epicentral receiver functions at site A21 filtered below 1 Hz. Red triangles represent the receiver locations relative to the profile. Red line at 0 s indicates the first recorded P-wave motion. Green and orange (where present) circles indicate relative time delay of the positive Ps phases likely derived at the crust-manltle interface. A) Back-azimuth ranges between 300°-350°. B) Back-azimuth ranges between 020°-080°. C) Back-azimuth ranges between 170°-200°.

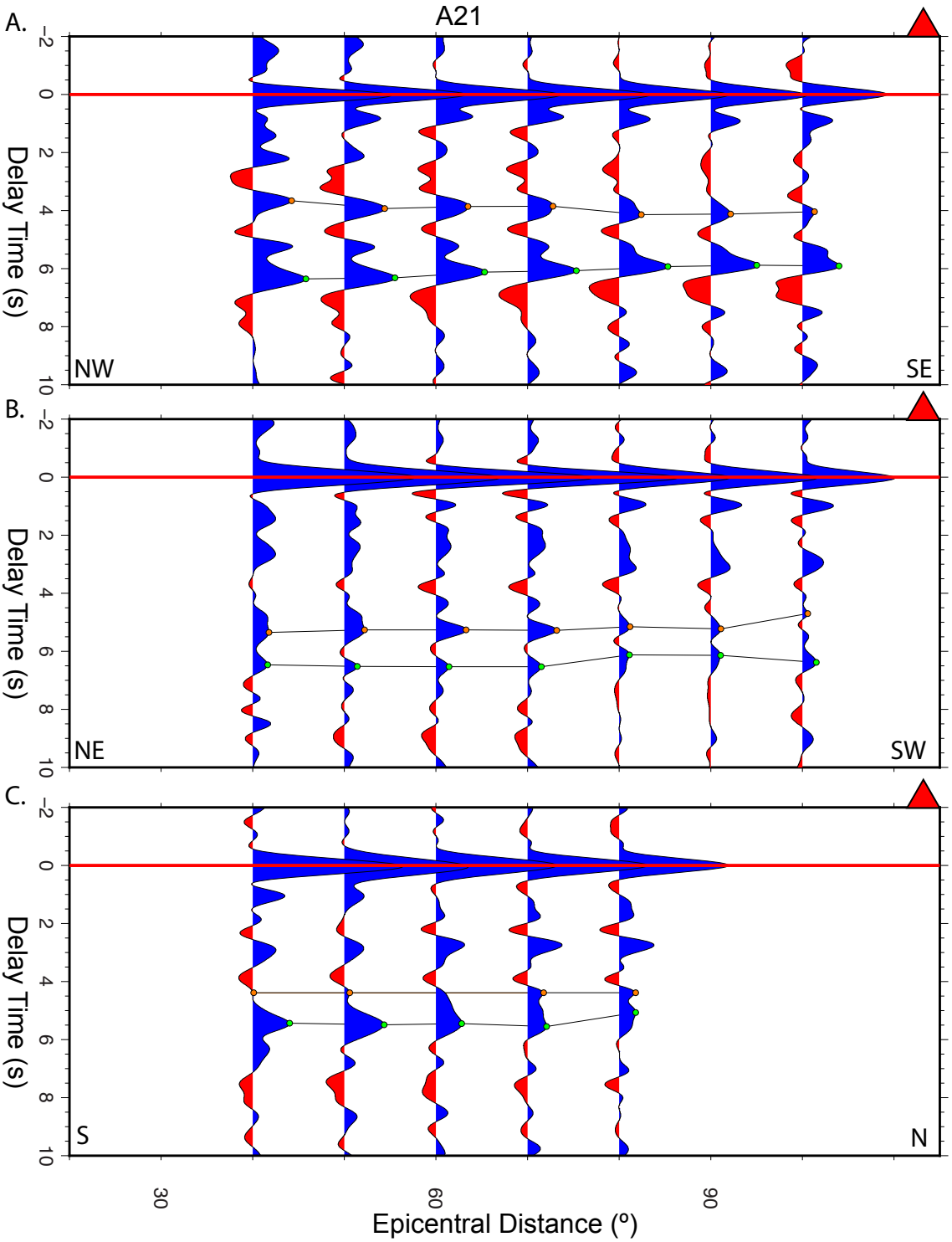


Figure 24: Interpreted epicentral receiver functions at site A21 filtered below 2 Hz. Red triangles represent the receiver locations relative to the profile. Red line at 0 s indicates the first recorded P-wave motion. Green and orange circles and indicate relative time delay of the positive Ps phases likely derived at the crust-manltle interface. A) Back-azimuth ranges between 300°-350°. B) Back-azimuth ranges between 020°-080°. C) Back-azimuth ranges between 170°-200°.

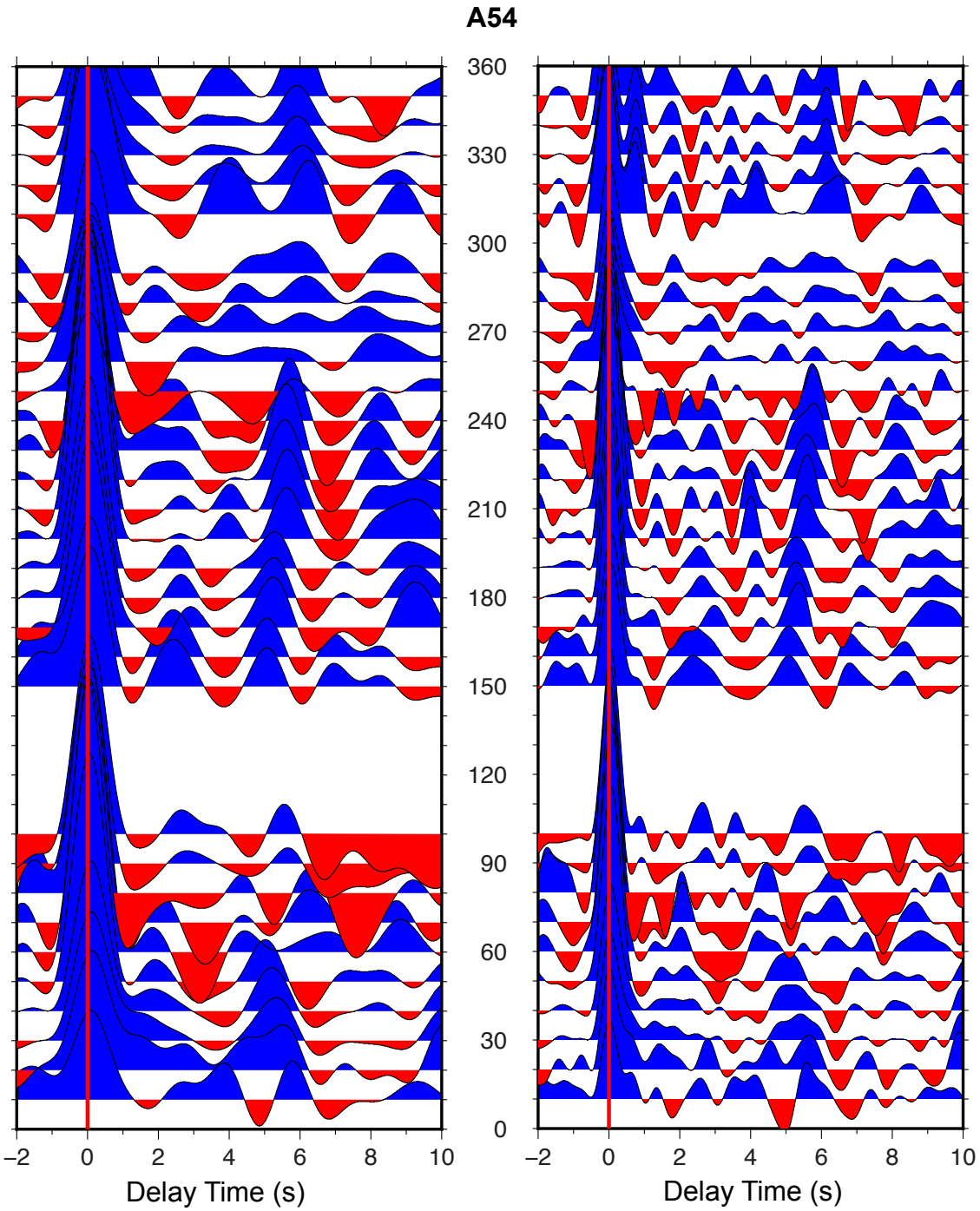


Figure 25: Back-azimuth reciever function gathers at site A54. The x-axis is delay time in seconds and the y-axis is event back-azimuth direction from 0°-360°.Reciever functions are filtered below 1 Hz (left) and 2 Hz (right). The red line set at 0 s indicates initial P-wave motion. No data were present between for back-azimuths 090°-140°.

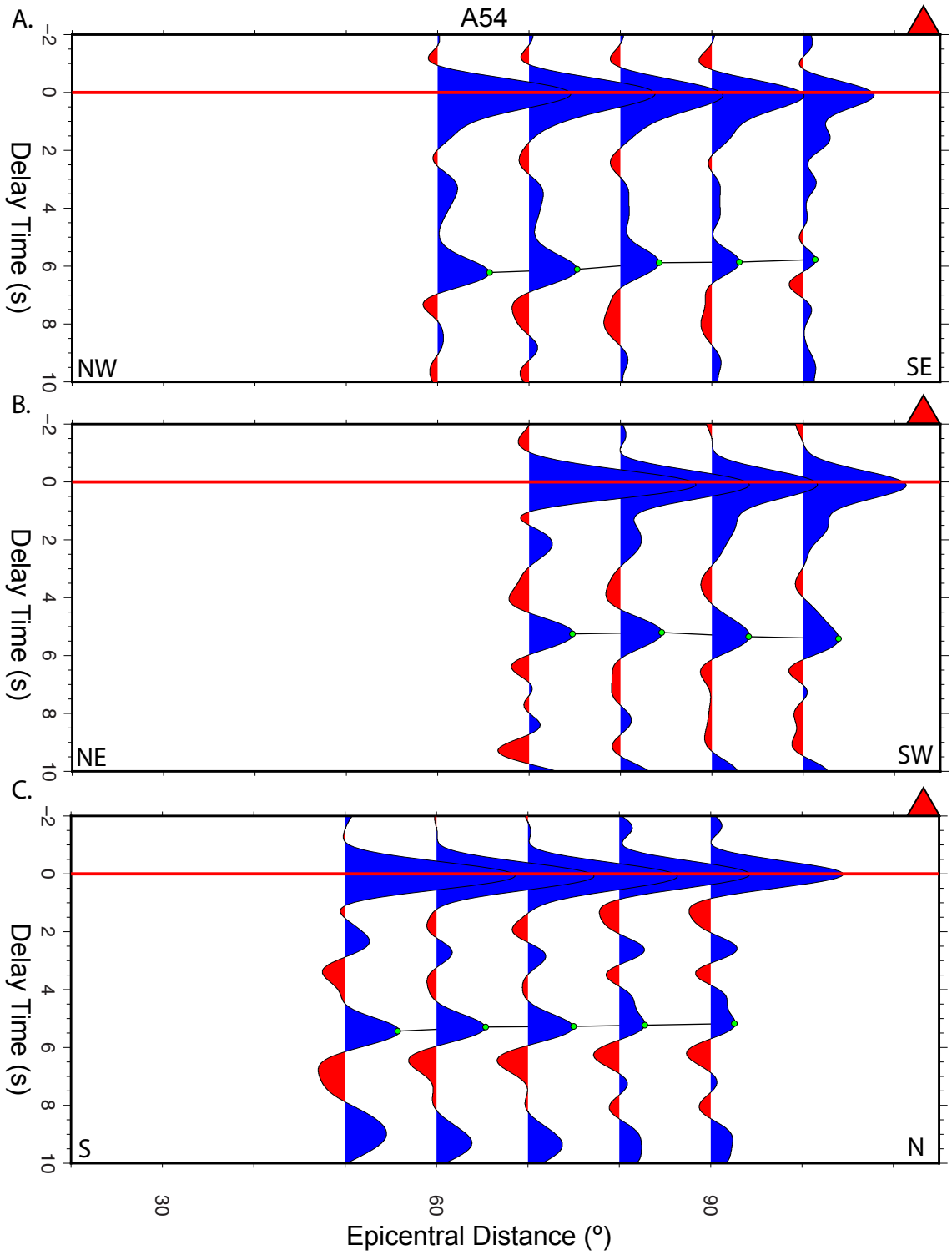


Figure 26: Interpreted epicentral receiver functions for site A54 filtered below 1 Hz. Red triangles represent the receiver locations relative to the profile. Red line at 0 s indicates the first recorded P-wave motion. Green circles indicate relative time delay of the positive phase interpreted as the Moho derived Ps phase. A) Back-azimuth ranges between 300°-350°. B) Back-azimuth ranges between 030°-050°. C) Back-azimuth ranges between 180°-190°.

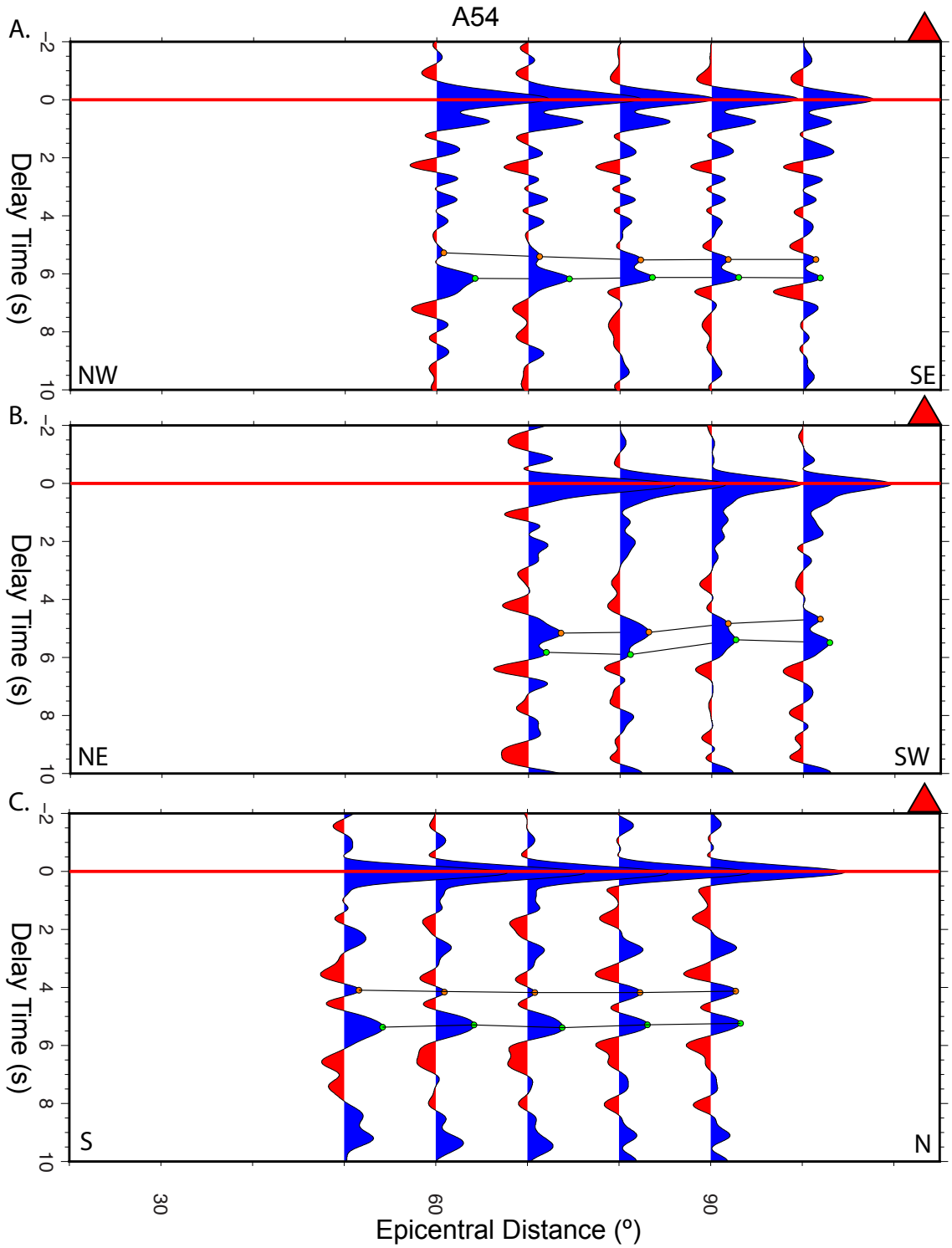


Figure 27: Interpreted epicentral receiver functions for site A54 filtered below 2 Hz. Red triangles represent the receiver locations relative to the profile. Red line at 0 s indicates the first recorded P-wave motion. Green and orange circles indicate relative time delay of the positive Ps phases likely derived at the crust-manltle interface. A) Back-azimuth ranges between 300°-350°. B) Back-azimuth ranges between 030°-050°. C) Back-azimuth ranges between 180°-190°.

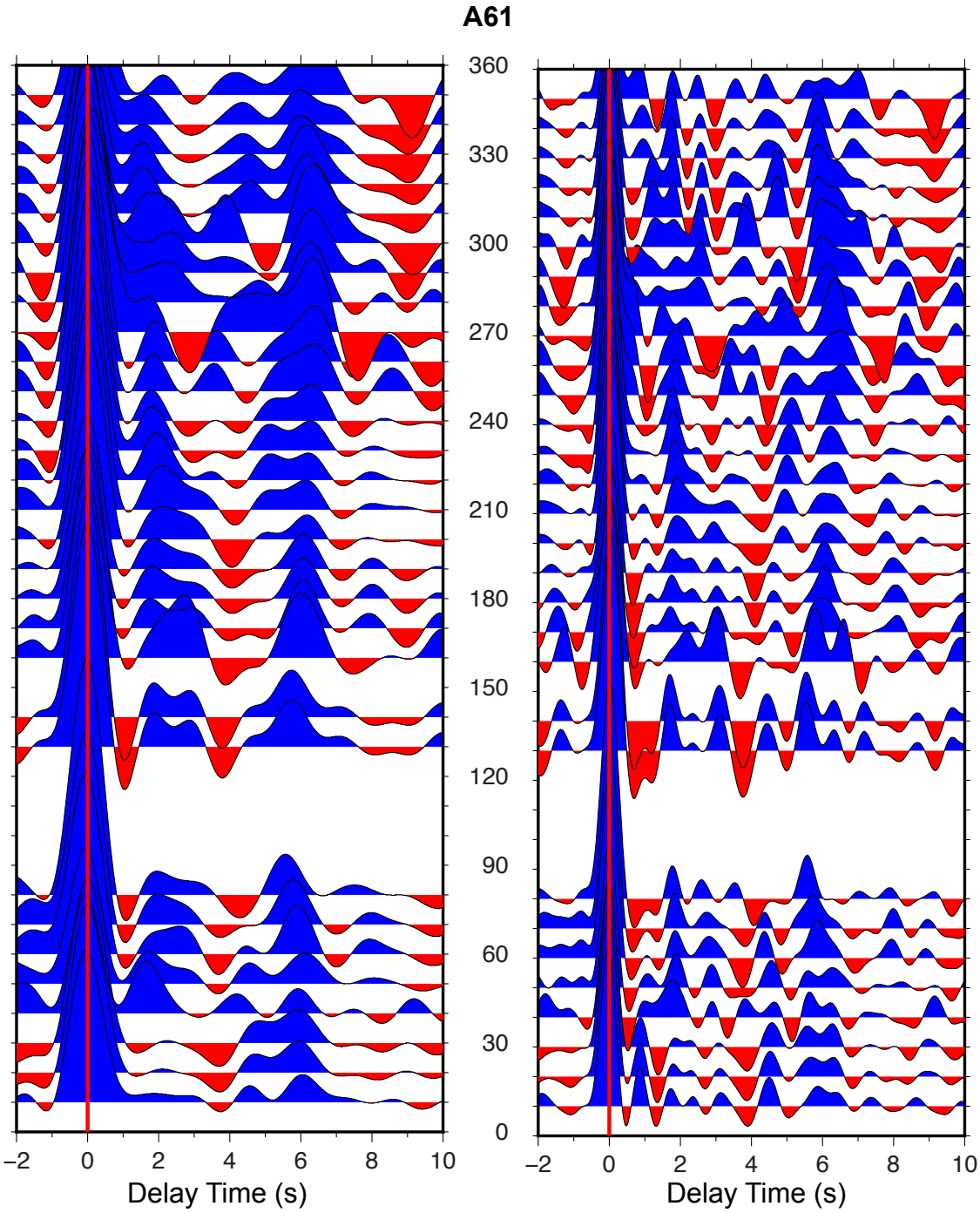


Figure 28: Back-azimuth reciever function gathers at site A61. The x-axis is delay time in seconds and the y-axis is event back-azimuth direction from 0°-360°.Reciever functions are filtered below 1 Hz (left) and 2 Hz (right). The red line set at 0 s indicates initial P-wave motion. No data were present between for back-azimuths of 150° and 90°-120°.

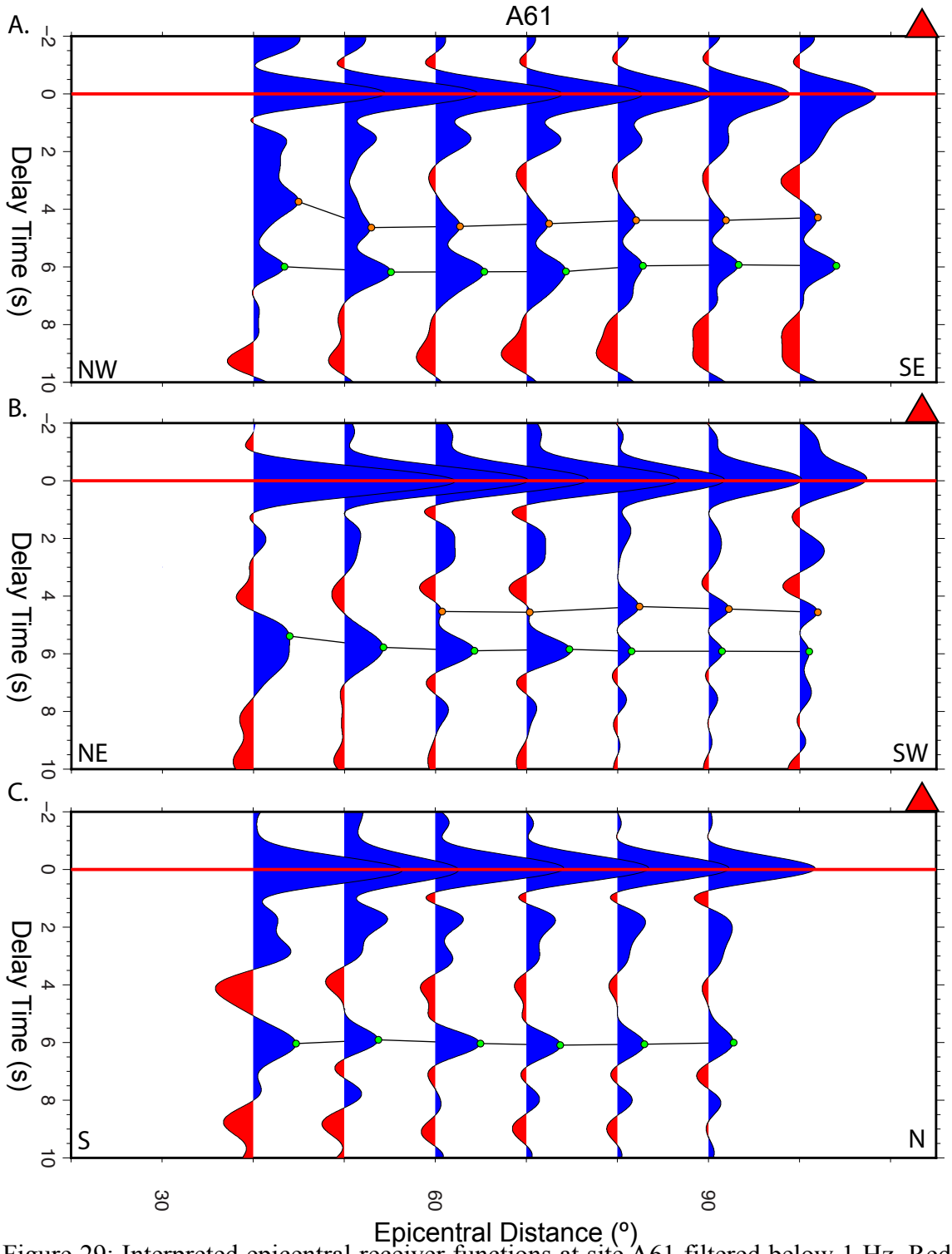


Figure 29: Interpreted epicentral receiver functions at site A61 filtered below 1 Hz. Red triangles represent the receiver locations relative to the profile. Red line at 0 s indicates the first recorded P-wave motion. Green and orange (where present) circles indicate relative time delay of the positive Ps phases likely derived at the crust-manltle interface. A) Back-azimuth ranges between 310°-340°. B) Back-azimuth ranges between 020°-080°. C) Back-azimuth ranges between 170°-190°.

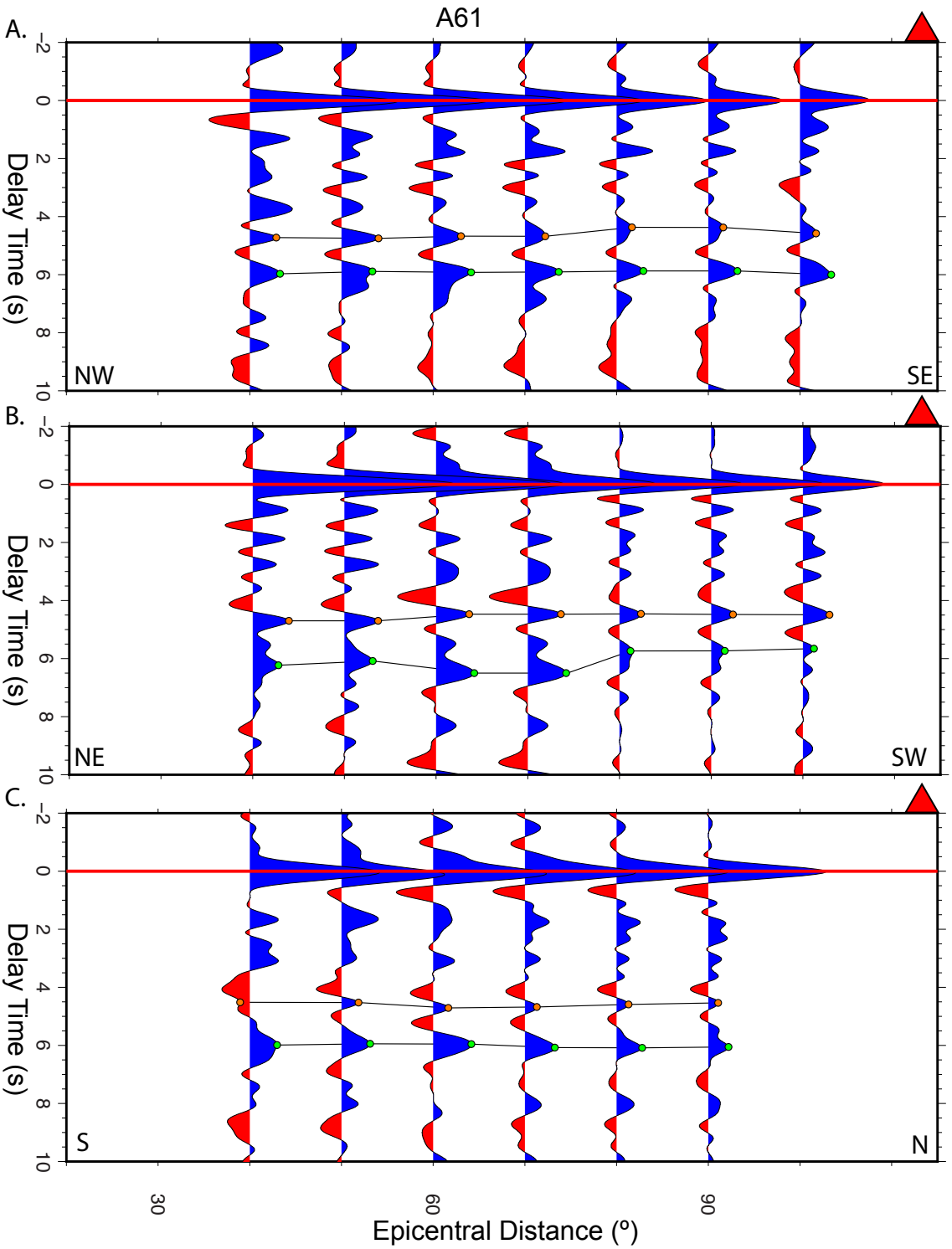


Figure 30: Interpreted epicentral receiver functions at site A61 filtered below 2 Hz. Red triangles represent the receiver locations relative to the profile. Red line at 0 s indicates the first recorded P-wave motion. Green and orange circles indicate relative time delay of the positive Ps phases likely derived at the crust-manltle interface. A) Back-azimuth ranges between 310°-340°. B) Back-azimuth ranges between 020°-080°. C) Back-azimuth ranges between 170°-190°.

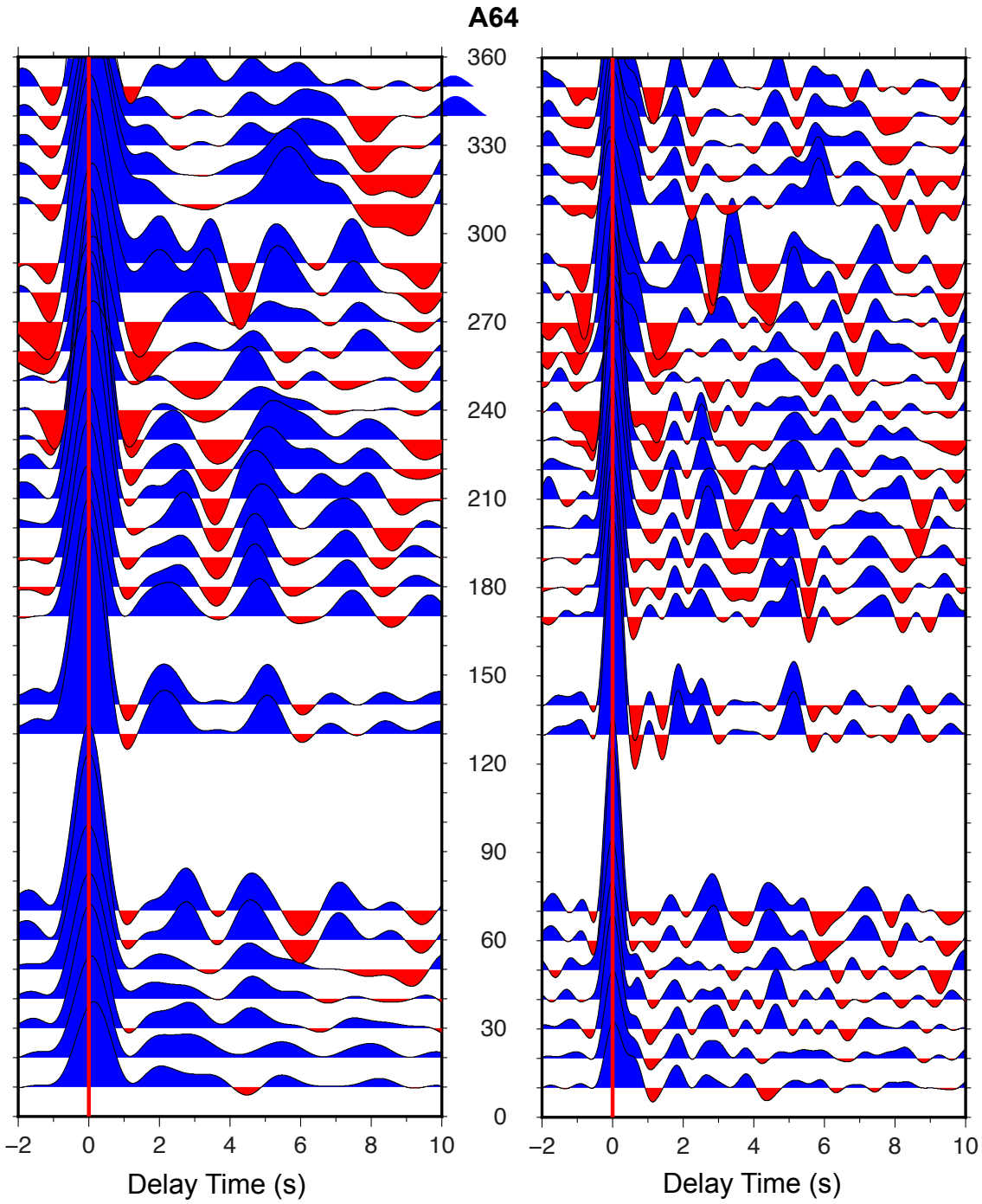


Figure 31: Back-azimuth reciever function gathers at site A64. The x-axis is delay time in seconds and the y-axis is event back-azimuth direction from 0°-360°.Reciever functions are filtered below 1 Hz (left) and 2 Hz (right). The red line set at 0 s indicates initial P-wave motion. No data were present between for back-azimuths of 300°, 150°-160°, and 90°-120°.

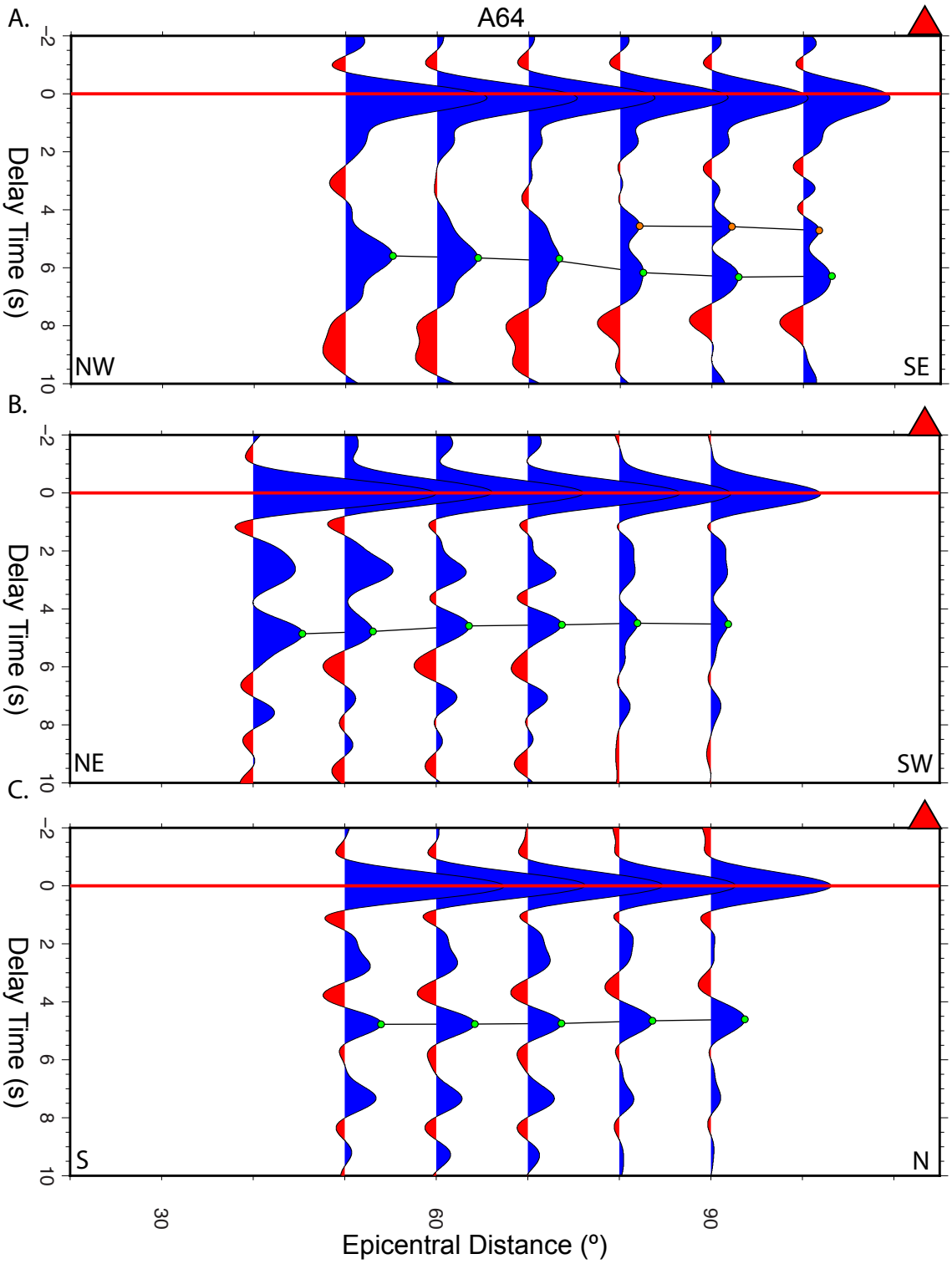


Figure 32: Interpreted epicentral receiver functions for site A64 filtered below 1 Hz. Red triangles represent the receiver locations relative to the profile. Red line at 0 s indicates the the first recorded P-wave motion. Green and orange (where present) circles indicate relative time delay of the positive Ps phases likely derived at the crust-manltle interface. A) Back-azimuth ranges between 310°-340°. B) Back-azimuth ranges between 010°-065°. C) Back-azimuth ranges between 170°-190°.

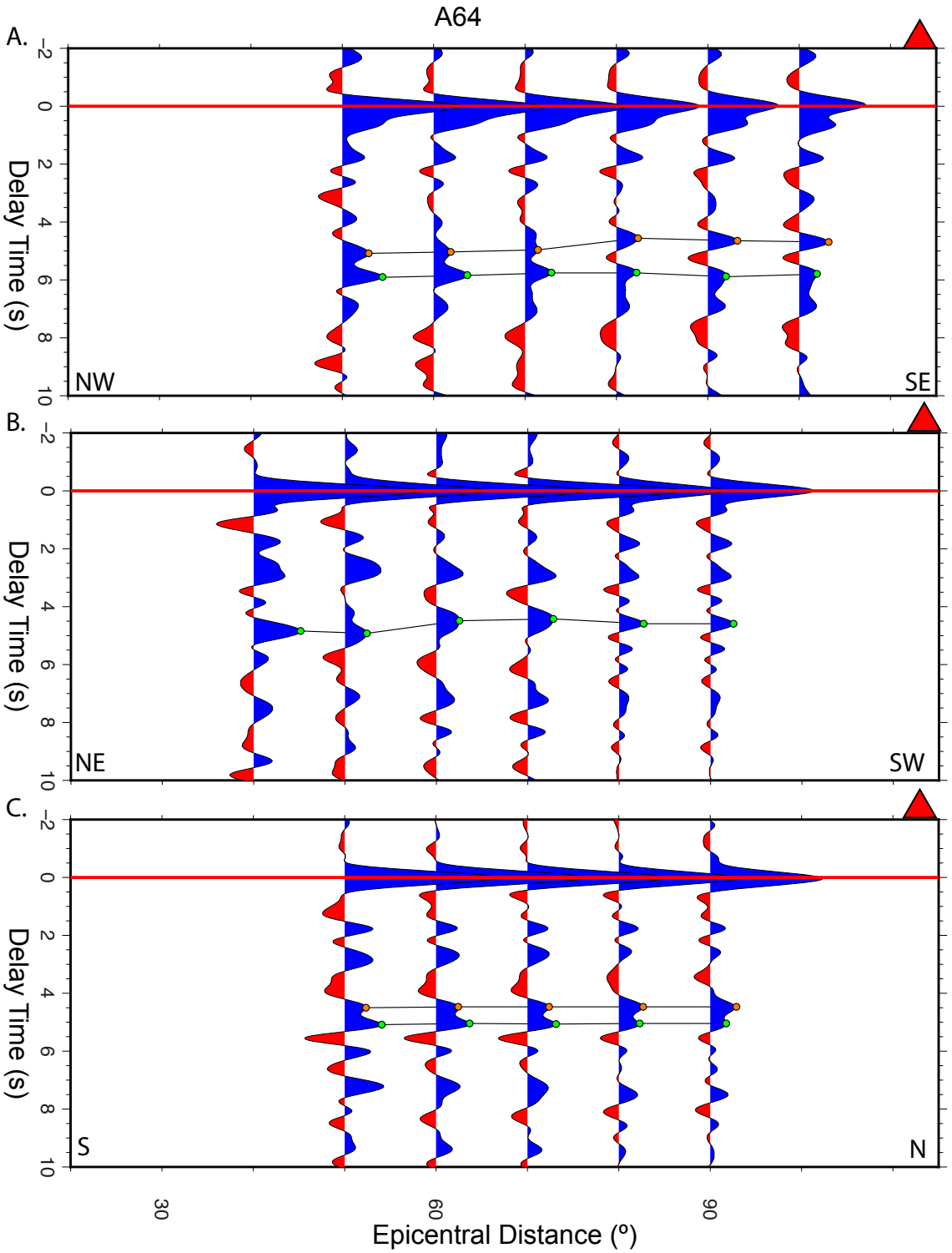


Figure 33: Interpreted epicentral receiver functions for site A64 filtered below 2 Hz. Red triangles represent the receiver locations relative to the profile. Red line at 0 s indicates the the first recorded P-wave motion. Green and orange circles indicate relative time delay of the positive Ps phases likely derived at the crust-manltle interface. A) Back-azimuth ranges between 310°-340°. B) Back-azimuth ranges between 010°-065°. C) Back-azimuth ranges between 170°-190°.

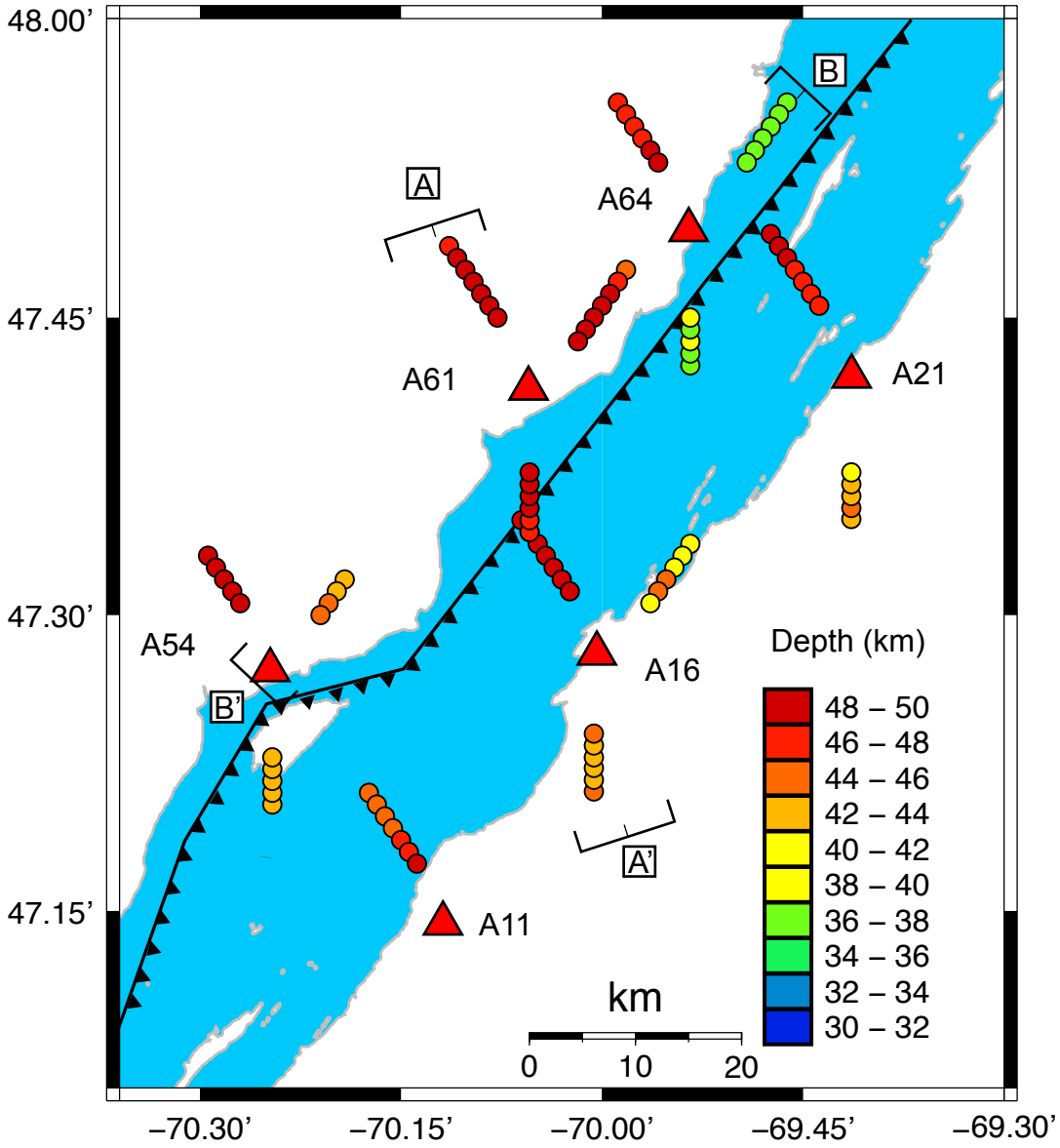


Figure 34: Depth estimate map of single pulses and late arrival of double pulses. produced from Ps phases in 1hz receiver functions and late Ps phase where double pulses are present in 2 Hz receiver functions. Sites where the late Ps phase arrival were interpreted in the 2 Hz receiver functions are A61, A64, and A21. The NW directed profile produced double phases at all sites mentioned above. The NE directed profile at site A61 also produced a double pulse. The Appalachian Front is indicated by the solid toothed black line.

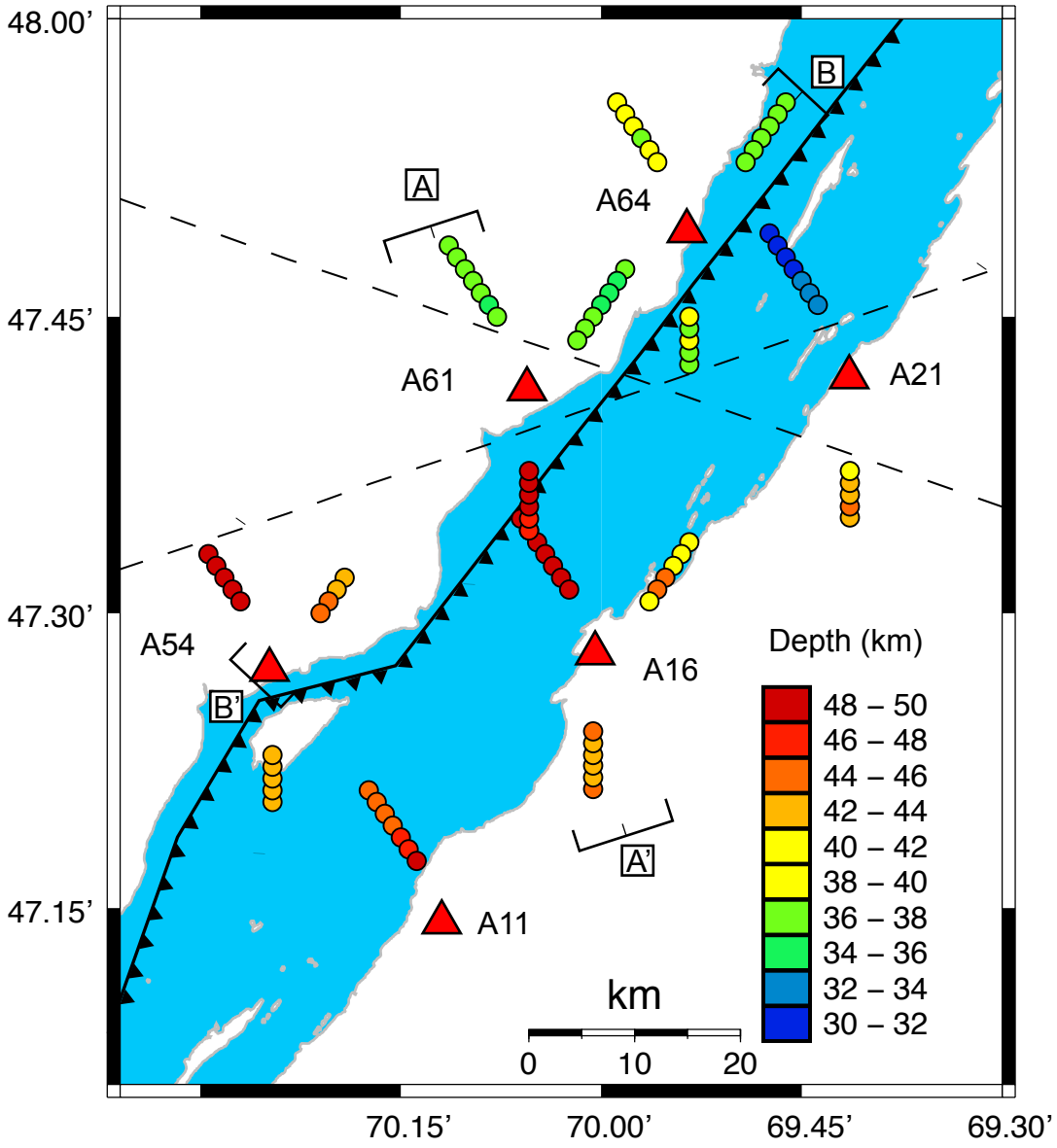


Figure 35: Depth estimate map of single pulses and early arrival of double pulses. produced from Ps phases in 1hz receiver functions and late Ps phase where double pulses are present in 2 Hz receiver functions. Sites where the early Ps phase arrival were interpreted in the 2 Hz receiver functions are A61, A64, and A21. The NW directed profile produced double phases at all sites mentioned above. The NE directed profile at site A61 also produced a double pulse. The Appalachian Front is indicated by the solid toothed black line. The dashed line indicates the orientation of the hypothetical shear zone.

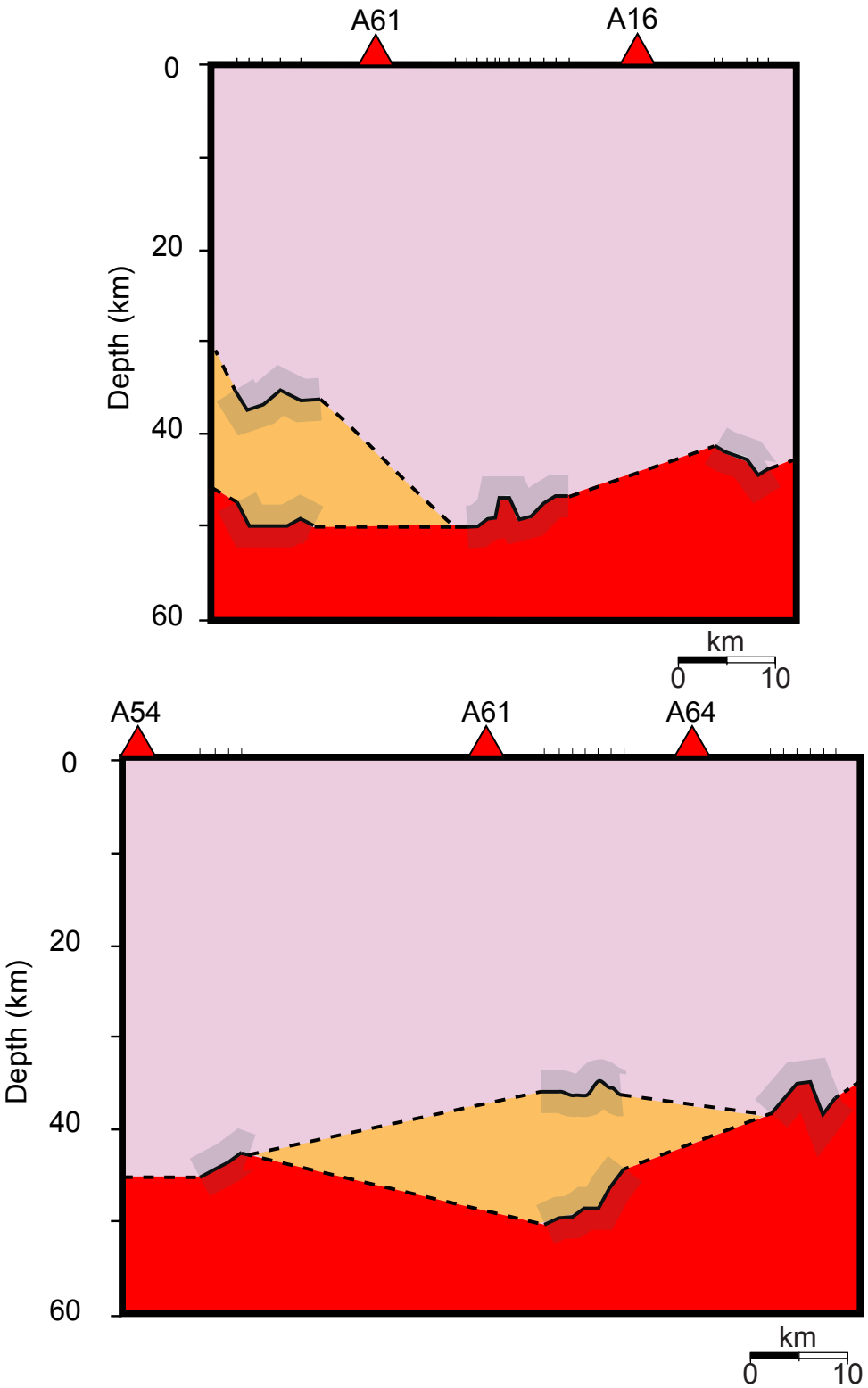


Figure 36: Cross-sections across (A) and along (B) the Appalachian Front. Tick marks along the upper horizontal axis indicate pierce point projections to the profile. Solid lines represent depth estimates from receiver functions, shaded area shows depth estimate error. Dashed lines represent inferred Moho depths A) Shows A to A' profile on Figs. 34 & 35. B) Shows B to B' profile from Figs. 34 & 35.